Logic-Based Modeling of Inflammatory Macrophage Crosstalk with Glomerular Endothelial Cells in Diabetic Kidney Disease

Krutika Patidar[1,*] and Ashlee N. Ford Versypt[1,†]

[1] *Department of Chemical and Biological Engineering, University at Buffalo, The State University of New York, Buffalo, NY 14260, United States*

Diabetic kidney disease is a complication in 1 out of 3 patients with diabetes. Aberrant glucose metabolism in diabetes leads to an immune response causing inflammation, which leads to structural and functional damage in the glomerular cells of the kidney. Complex cellular signaling lies at the core of metabolic and functional derangement. Unfortunately, the mechanism underlying the role of inflammation on glomerular endothelial cell dysfunction in diabetic kidney disease is not fully understood. Computational models in systems biology allow the integration of experimental evidence and cellular signaling networks to understand mechanisms involved in disease progression. To address the knowledge gap, we built a logic-based differential equations model to study macrophage-dependent inflammation in glomerular endothelial cells during diabetic kidney disease progression. We studied the crosstalk between macrophages and glomerular endothelial cells in the kidney using a protein signaling network stimulated with glucose and lipopolysaccharide. The network and model was built using an open-source software package Netflux. This modeling approach overcomes the complexity of studying network model and the need for extensive mechanistic details. The model simulations were trained and validated against available biochemical data from *in vitro* experiments. We used the model to identify the mechanisms responsible for dysregulated signaling in both macrophages and glomerular endothelial cells during diabetic kidney disease. Our model findings contribute to the understanding of signaling and molecular perturbations on glomerular endothelial cell morphology in early stage of diabetic kidney disease.

* krutikap@buffalo.edu

† ashleefv@buffalo.edu

I. INTRODUCTION

Diabetic kidney disease (DKD) is a major microvascular complication in the kidney that affects about 30% of patients with type I diabetes and approximately 40% of patients with type II diabetes [1]. DKD causes reduced kidney function and may progress into chronic kidney disease (CKD) and end-stage renal disease (ESRD), which imposes a high burden on the cost of living and quality of life. High mortality associated with diabetes is largely confined to patients with CKD complications [2]. Reports suggest that approximately 12-55% of ESRDs are due to diabetes [3]. Although diabetes management is one of the preventative treatments for DKD [4], the rising number of cases of type 1 and type 2 diabetes continue to increase the risk of DKD prevalence [1]. There is still an urgent need to better understand the pathophysiology of DKD through effective and preventative treatment strategies that can mitigate early signs of microvascular damage and DKD prevalence in diabetic patients [5].

Ongoing research suggests that DKD is caused by many complex and interlinked processes associated with high blood glucose and poor glycemic control. The hyperglycemic microenvironment has been linked to metabolic dysfunction in immune cells and inflammation. The microenvironment influences the activation of a pro-inflammatory stimulus such as lipopolysaccharide (LPS), interferon-gamma (IFN-γ), or tumor necrosis factor (TNF) [6, 7], which in turn increases glucose uptake in immune cells [8]. In the early stage of DKD development, immune cells like macrophages tend to polarize to a pro-inflammatory phenotype over an anti-inflammatory phenotype [8, 9]. Together, the synergic action of pro-inflammatory mediators and increased glucose uptake contributes to dysregulated immune response and signaling [8]. This dysregulated signaling enhances the expression of pro-inflammatory molecules such as IL-6, TNF-α, IL-1β, and reactive oxygen species (ROS), which affect downstream macrophage response and activity [8, 9]. Studies showed that these circulating pro-inflammatory molecules infiltrate the glomerular interstitium in the diabetic kidney [10] and cause microvascular damage to the glomerulus [6, 11]. Recruitment of inflammatory macrophages and their mediators is an important step in the pathophysiology of the early stage of DKD [10]. We only have a superficial understanding of the highly complex and diverse molecular interactions in the diabetic kidney [6]. Hence, a deeper analysis of glucose-mediated inflammatory mechanisms and pathways in the diabetic kidney can contribute to a comprehensive understanding of DKD development and progression.

Glomerular endothelial dysfunction is a pathological phenomenon that can characterize the early stages of DKD development and progression. In the functional unit of the kidney, glomerular endothelial cells (GEC) are one of the early targets of diabetes-dependent inflammation and injury [3]. Numerous studies suggest that activation of GECs in early DKD can dysregulate signaling pathways, promote intracellular hyperglycemia, elevate AGEs and their receptors, affect cell-cell adhesion, glomerular permeability, and promote recruitment of inflammatory molecules [12]. LPS stimulated pro-inflammatory macrophages are involved in activation of GECs *in vitro* [13]. The inflammatory mediators and immune cells disrupt vascular endothelial growth factor (VEGF) expression, which plays a central role in maintaining GEC vascular function and nitric oxide (NO) homeostasis [14, 15]. Imbalanced VEGF expression causes uncoupling of endothelial nitric oxide synthase (eNOS), NO imbalance, and loss of endothelial barrier integrity [14].

The uncoupling of eNOS causes eNOS to produce NO as a main product as well as ROS as by-product, which leads to excessive oxidation of NO and reduces NO bioavailability in GECs [16]. Hence, uncoupling of eNOS is an important indicator of GEC activation and dysfunction. NO bioavailability within GECs has been associated with glomerular endothelial permeability [17, 18]. About 50% of the filtration through the glomerulus is dependent on GECs and the endothelial cell surface layer, which makes GECs an essential contributor to the glomerular permeability of the kidney [19]. The permeability of GECs is dependent on the intercellular endothelial fenestrations or gaps, which are regulated by junction proteins on the surface of GECs. Biophysical models also showed that the spatial arrangement of these GEC fenestrations is relevant to the overall glomerular filtration rate of the kidney [20–22]. An experimental study suggested a potential link between NO bioavailability and endothelial junction proteins, which modulates the endothelial cell barrier integrity [23]. Thus, changes in GEC fenestration width and density are markers of GEC dysfunction during DKD progression. Despite experimental studies on GECs in both normal and diseased state, a direct mechanistic link between macrophage-dependent endothelial cell activation and dysfunction in the early stage of DKD are not fully understood [23].

In the present study, we built a protein signaling network (PSN) of interconnected pathways between two cell types, macrophages, and GECs, to study glucose-mediated inflammatory mechanisms in DKD. A PSN depicts relationship between interacting proteins using directional arrows [24]. We used a computational approach to integrate published experimental evidence and protein signaling networks. However, signaling networks with a large number of interacting species can become complex and tedious to model. Often, ordinary differential equations (ODE) are used to model these biochemical networks but these models rely on extensive data and parameter values as well as knowledge of reaction kinetics. Alternatively, modelers have used techniques like logic-based modeling, fuzzy logic modeling, and extreme pathways analysis to study complex signaling networks [24, 25]. These techniques require few or no parameters. For instance, a discrete logic model (Boolean model) successfully showed the changes in endothelial cell behavior and signaling due to extracellular micro-environments [26]. A logic-based model (LBM) was used to gain qualitative understanding of species expression, signaling pathways, and missing interactions involved in T cell activation [27]. Furthermore, pathway analysis of differentially expressed genes and profiles in early DKD has been quite useful in understanding important pathophysiologic factors in DKD [28]. However, each of these approaches have their limitations including limited prediction of continuous dynamics in Boolean models, lack of realistic timescales in fuzzy logic analysis, and extensive data collection for pathway analysis. We are interested in predicting continuous signaling dynamics with limited available data and mechanistic details. Therefore, we apply a modeling technique proposed by Kraeutler *et al.* that combines continuous and dynamic ODE models with qualitative LBMs [24, 25]. Kraeutler *et al.* presented the advantages of using this ODE-type LBM, especially in the lack of mechanistic parameters and details. Their ODE-type LBM identified unexpected network relationships, generated experimentally testable predictions, and agreed with findings from a validated biochemical model [25]. Therefore, we applied this ODE-type logic-based modeling approach to our PSN between macrophage and GECs stimulated under different conditions. To our knowledge, an analysis of signaling crosstalk between macrophages and GECs using ODE-type logic-based

modeling technique hasn't been done previously. We predicted species dynamics, network relationships, and key drivers of macrophage-dependent inflammation and glomerular endothelial dysfunction in the early stage of DKD.

The article has been organized as follows. We explain the rationale behind the choice of species and pathways in the proposed network, steps in model development and simulation, and experimental data selection in Section II. We provide the results from model simulation, validation, and predictions in Section III. The relevant conclusions from this study are summarized in Section IV. The appendix Section A provides supplementary information and model parameters used in this study.

II. METHODS

A. Network Assembly

The PSN (Fig. 1) was formulated and assembled using literature studies and pathway databases [6, 8, 14, 16, 26, 29–37]. The PSN captures the signaling pathways and molecules that cause inflammation and dysfunction in two cell types i.e. macrophages and GECs. Considering the complex nature of these interactions, we included signaling pathways involved in two main events in early DKD. These events include the release of pro-inflammatory molecules due to pro-inflammatory macrophages and macrophage-dependent GEC activation and dysfunction. The rationale behind these pathways and molecules is discussed later in this section. There are 30 species nodes and 40 interaction edges in the multi-cellular PSN (Fig. 1). The green nodes are inputs or stimuli, white nodes are regulatory nodes, and blue nodes are model responses. The network has two stimuli, glucose, and LPS. The network was stimulated with three different treatment conditions i.e. glucose only (GLU), LPS only (LPS), and glucose and LPS. The edge connection governs activating or inhibiting interaction between two species. Based on the logic-based formalism, two or more incoming edges are connected by an OR logic rule except where stated by a red circle denoting an AND logic rule (Fig. 1). OR logic rule between two input nodes suggests that either input can activate or inhibit the output node. AND logic rule between two input nodes suggests that all inputs must be present to activate or inhibit the output node.

In diabetes, immune cells like macrophages fail to metabolize glucose or regulate efficient transport of glucose, which leads to intracellular hyperglycemia. Studies showed that this microenvironment initiates a pro-inflammatory signaling response downstream, which is governed by activation of LPS and toll-like receptors such as TLR4 [8, 9]. In cell culture experiments, bacterial LPS is a representative pathogen-associated molecular pattern (PAMP) that allows mammalian cells to recognize bacterial invasion and trigger innate immune responses. In cultured macrophages, LPS is used to stimulate a strong inflammatory response, which can mimic glucose-mediated inflammation in macrophages [8]. Hence, LPS was considered as one of the stimuli. LPS transduction signal is carried by activation of PI3K and Akt kinases, which mediate macrophage response, energy consumption, and energy metabolism [38]. Akt is a primary substrate of PI3K and is associated with the regulation of inflammatory and energetic metabolic responses. Therefore, we hypothesize that PI3K and Akt play an important role in macrophage polarization in our network [8].

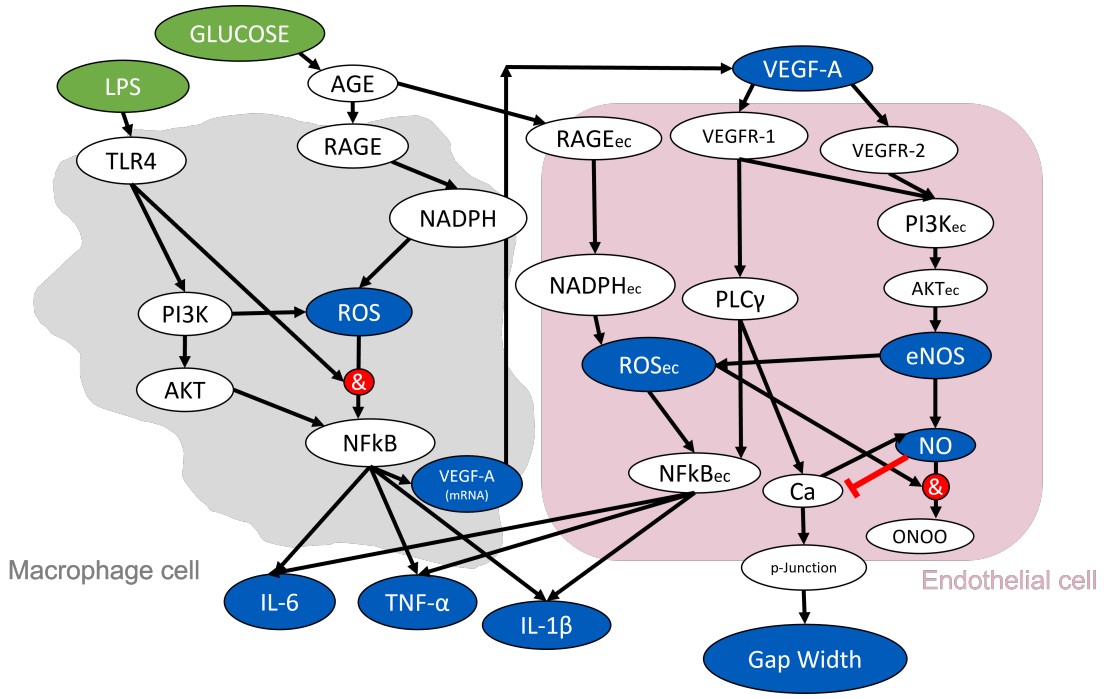

FIG. 1. A representation of multi-cellular protein signaling network of crosstalk between macrophages (left) and glomerular endothelial cells (right) stimulated with glucose and lipopolysaccharide (LPS), a pro-inflammatory stimulus. Green nodes (ovals) are input nodes, blue nodes are output nodes, and white nodes are regulatory nodes. Black arrows (edges) are activating interaction, red line with a dash at the end is an inhibiting interaction, and red circles are logic AND gates. An OR logic rule connects two or more edges to a subsequent node throughout the network unless stated otherwise by an AND logic gate. The subscript "ec" denotes an intracellular species expressed in endothelial cells. IL-6, TNF-α, IL-1β, and VEGF-A are protein levels that are expressed in extracellular space. ROS, ROSec, VEGF-A (mRNA), and NO are expressed within the cells. Gap Width node denotes fractional change in fenestration size between adjacent glomerular endothelial cells. The phosphorylated junction protein levels are represented by $pJunction$ node.

Advanced glycation is one of the major pathways involved in the development and progression of different diabetic complications including DKD [37]. This protein glycation leads to adavanced glycation end products (AGE), which activate and modify intracellular pathways through receptor mediated signaling [37]. Expression of receptors of AGE (RAGE) is enhanced in certain cells like macrophages and endothelial cells during diabetes and inflammation. AGE and RAGE interaction on macrophages causes oxidative stress and activation of nuclear factor-κB (NF-κB) [37]. Glycated proteins release ROS via activation of NADPH oxidase [32, 39]. Moreover, aberrant PI3K-Akt signaling increases ROS levels through either direct modulation of mitochondrial bioenergetics or indirect production of ROS as a metabolic by-product [40]. Hence, NADPH and PI3K-dependent ROS were considered in our network to gain a better perspective on mediators of ROS. Further, transcription factor NF-κB contributes to the structural and functional changes observed in DKD, including pro-inflammatory macrophage polarization [37]. NF-κB is responsible for expression of pro-inflammatory cytokines like IL-6, TNF-α, and IL-β, inflammatory markers, growth factors, and adhesion molecules [6]. The expressed inflammatory cytokines and VEGF-A were associated with direct or indirect activation of endothelial cells in our network.

Macrophage-dependent VEGF-A expression is associated with the direct activation of GECs in our network. VEGF expression modulates the crosstalk between endothelial cells and macrophages [41]. VEGF and its isoforms are critical

to GECs. Excess VEGF contributes to DKD develpoment and progression through disrupted signaling in GECs, whereas low VEGF levels can result in loss of capillaries and endothelial cells in the glomerulus [42]. VEGF expression promotes endothelial cell development through NO modulation [42]. Studies suggested that glucose indirectly regulates VEGF-A and its receptor (VEGFR-1 and VEGFR-2) signaling in GEC [41, 43, 44]. Shibuya discussed the role of VEGFR-1 receptor as a positive regulator of inflammation and immune cell recruitment via PLC-γ/PKC pathway [34]. The downstream signaling of VEGFR-1 is not fully understood mainly due to its mild biological activity in culture [34]. VEGF-A mediates signal transduction for cell proliferation, survival, migration, and enhanced vascular permeability via VEGFR-2 receptor [15]. VEGFR-2-dependent signaling promotes eNOS activity, which produces NO, an important vasodilator in GECs [15]. VEGF-A and VEGFR-2 activity was shown to have reduced in the GEC in diabetes [45]. This phenomenon leads to perturbations in downstream signaling, eNOS uncoupling, and reduced NO bioavailability [46]. As a result, excess ROS in GECs can react with available NO to form reactive nitrogen species like peroxynitrite ($ONOO$) [42, 47]. In our network, the VEGF-dependent signaling pathway accounted for VEGF-A receptors ($VEGFR_1$ and $VEGFR_2$), PLC-γ, eNOS, NO, ROS, and reactive nitrogen species expression. We also connected VEGF-dependent NO bioavailability with GEC dysfunction. We considered cell-cell junction proteins that hold adjacent GECs together, which modulate the passage of macromolecules, proteins, or infiltrating macrophages through the GEC layer. In activated GECs, the phosphorylation of these junction proteins such as VE-cadherin is regulated by calcium (Ca) expression via the PLC-γ pathway and NO expression [18, 48]. The phosphorylation of VE-cadherin triggers the opening of the junction between adjacent GECs, shown as $p-Junction$ node in our network. We hypothesized that the junction opening or closing is directly related to the size of endothelial cell fenestration, shown as Gap Width node in the network.

B. Continuous ODE-type Logic-based Model

We modeled the PSN using a continuous ODE-type LBM. This ODE-type logic-based modeling technique combines the continuous and dynamic ODE models with the qualitative LBMs using normalized hill functions. This modeling technique was proposed by Kraeutler *et al.* [25]. These equations were generated in the NetFlux software package upon providing the necessary interaction rules and species list [25]. Netflux package compiled these model equations and default parameters as MATLAB scripts, which was exported and used to run the model. These equations are dependent on reaction parameters (W, n, EC_{50}) and species parameters (τ, y_0, $y_{\max}$), as shown from a subset of equations in the Fig. 2, eq. (1)-(4) [25]. The network model equations and corresponding interaction rules can be found in the supplementary file (Appendix A 1). The model inputs (i.e. glucose or LPS) can hold a discrete value of 0 or 1 based on whether input is inactive or fully active, respectively. The model species can have a value between 0 and 1. Each species or node is activated or inhibited by the previous node based on the interaction rule computed with a normalized-Hill function. Each equation has a source term and degradation term. In eq. (1), the first term depicts activation of $TLR4$ by LPS via a normalized Hill-type activation function, and second term depicts degradation of

$TLR4$ divided by time constant τ parameter.

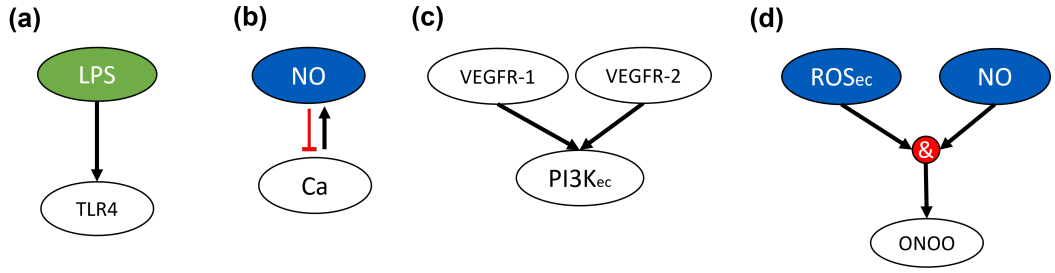

FIG. 2. Logic based formalism for a protein signaling network (PSN). The above shown species interactions (a)-(d) are used to explain logic-based model equations for the PSN. (a) LPS activates $TLR4$. (b) NO inhibits Calcium (Ca) and Ca activates NO. (c) $VEGFR_1$ and $VEGFR_2$ activate $PI3K_{ec}$ using an OR logic rule. (d) ROS_{ec} and NO activate $ONOO$ using an AND logic rule. Black arrow is activating interaction, red line with a dash at the end is an inhibiting interaction, and red circle is a logic AND gate.

$$\frac{\mathrm{dTLR4}}{\mathrm{dt}} = \frac{y_{\mathrm{max}_{\mathrm{TLR4}}} f_{\mathrm{act}}(\mathrm{LPS}) - \mathrm{TLR4}}{\tau_{\mathrm{TLR4}}} \tag{1}$$

In eq. (2), Ca is inhibited by NO, and Ca activates NO in a negative feedback loop. Therefore, Ca activity is computed using a normalized Hill-type inhibition function.

$$\frac{\mathrm{dCa}}{\mathrm{dt}} = \frac{y_{\mathrm{max}_{\mathrm{Ca}}} f_{\mathrm{inhib}}(\mathrm{NO}) - \mathrm{Ca}}{\tau_{\mathrm{Ca}}} \tag{2}$$

If a species is activated or inhibited by two or more species, an AND or OR logic operator was applied to the incoming interaction functions. In eq. (3), $PI3K_{ec}$ is activated by $VEGFR_1$ and $VEGFR_2$ such that either receptors can activate $PI3K_{ec}$. Therefore, an OR logic rule was applied to this interaction. In eq. (4), $ONOO$ is a reactive nitrogen species produced in presence of both ROS and NO species. Therefore, AND logic rule was applied to this interaction.

$$\frac{\mathrm{dPI3K_{ec}}}{\mathrm{dt}} = \frac{y_{\mathrm{max}_{\mathrm{PI3K_{ec}}}} OR(f_{\mathrm{act}}(\mathrm{VEGFR_1}), f_{\mathrm{act}}(\mathrm{VEGFR_2})) - \mathrm{PI3K_{ec}}}{\tau_{\mathrm{PI3K_{ec}}}} \tag{3}$$

$$\frac{\mathrm{dONOO}}{\mathrm{dt}} = \frac{y_{\mathrm{max}_{\mathrm{ONOO}}} AND(f_{\mathrm{act}}(\mathrm{NO}), f_{\mathrm{act}}(\mathrm{ROS_{ec}})) - \mathrm{ONOO}}{\tau_{ONOO}} \tag{4}$$

In eq. (1)-(4), $f_{\mathrm{act}}(X)$ is activation function for species X, as shown in eq. (5). $f_{\mathrm{inhib}}(X)$ is inhibition function for species X, as shown in eq. (6). X is species such as LPS, NO, $VEGFR_1$, $VEGFR_2$, ROS_{ec}. y_{max} is maximal

concentration of species. τ_Y is time constant for species Y. W_X is reaction weight of species X. n is Hill coefficient. EC_{50} is half effect. $OR(m,n)$ is an OR logical operator for input m and n, as shown in eq. (9). $AND(m,n)$ is an AND logical operator for input m and n, as shown in eq. (10).

$$f_{\text{act}}(X) = W\frac{\beta X^n}{K^n + X^n} \tag{5}$$

$$f_{\text{inhib}}(X) = W - f_{\text{act}}(X) \tag{6}$$

$$\beta = \frac{EC_{50}^n - 1}{2EC_{50}^n - 1} \tag{7}$$

$$K = (\beta - 1)^{1/n} \tag{8}$$

$$OR(m,n) = m + n - mn \tag{9}$$

$$AND(m,n) = mn \tag{10}$$

C. Model Parameters

The model equations have parameters that can be divided into two categories, reaction parameters and species parameters. Reaction parameters such as reaction weight W (constrained as $0 \leq W \leq 1$), half maximal effective concentration EC_{50} (constrained as $0 < EC_{50} < 1$), and Hill coefficient n (constrained as $1.4 \leq n \leq 5$) govern the interactions between species in our network [25]. For a given interaction, the reaction weight W denotes the fraction of activation or inhibition of output species [25]. EC_{50} is the fraction of input required to induce half-maximal effect on the output [25]. The Hill coefficient n denotes the sensitivity to changes in inputs, which can be considered as a shape factor in our model [49]. These reaction parameters define the normalized Hill activation or inhibition function f. This function is constrained as $f(0) = 0, f(1) = W, f(0.5) = 0.5W$ in NetFlux [25]. The species parameters such as time constant τ (constrained $0.01 \leq \tau \leq 20$), initial value y_0, and maximal fractional activation of species $y_{\max}$ describe the activity of a species in our network. Time constant (τ) parameter is an arbitrary time parameter. This parameter modulates the signal propagation during early or late events and provides a rough estimate of local dynamic behavior of the network [27]. $y_{\max}$ is set to 1 by default and suggests full activity of a species. $y_{\max}$ can be below or above a value of 1 to denote species knock-down or over-expression, respectively [25]. The default values for

these parameters, as generated by Netflux, are $W = 1, EC_{50} = 0.5, n = 1.4, \tau = 1, y_0 = 0, y_{\max} = 1$.

D. Model Simulation

The model was simulated with default reaction and species parameters, given in Table A1 and A2, for GLU, LPS, and GLU and LPS treatment conditions. However, these model predictions were only qualitative and could not fit to the published data. The model parameters are not available in literature, and not all parameters have a biochemical relevance like kinetic parameters or rate constants. For this reason we optimized the model parameters in the model training step by fitting our model to a training dataset. Instead of a rigorous parameter optimization, we first performed a local sensitivity analysis to identify a subset of parameters that affect the model response significantly. Reducing the parameter space enables a thorough exploration of the subspace of influential parameters and provides greater confidence in model predictions [50]. A local sensitivity analysis was performed using finite difference approximation to generate two-dimensional sensitivity matrices based on eq. (11). S_{ij} is a sensitivity coefficient for a given output species i, which was computed by introducing an infinitesimal perturbation in parameter j. ΔY_i is the change in output species i. ΔP_j is the change in parameter j. A perturbation of 0.1% was introduced one at a time in each parameter in the subset. We identified sensitive EC_{50}, n, τ, y_0, and W parameters with this approach. Our analysis involves time-dependent responses, which makes it difficult to rank-order sensitivities. Therefore, we used sensitivity coefficients computed at the end time point (48 hours) and chose the parameters within the 90th percentile of the calculated sensitivities.

$$S_{ij} = \frac{\Delta Y_i P_j}{Y_i \Delta P_j} \tag{11}$$

The sensitive model parameter subspace (Appendix Table A3) was optimized using a multi-start non-linear least squares parameter optimization technique. We scaled the model parameters between 0 and 1 using a min-max scalar before parameter optimization. The scaling of parameters reduces bias in optimization process and achieves faster optimization. Then, we sampled 100 parameter start values using Latin hypercube sampling technique [51]. Each subset of parameter start values was optimized using the *fmincon* estimator in MATLAB. *fmincon* minimizes the objective function, which is the sum of squared error (SSE) between model prediction and published data (Section II E). Additionally, we calculated the parameter uncertainty using the Hessian matrix, which is an output argument from *fmincon* [52]. Hessian matrix provides the second order derivatives of the objection function. The variance-covariance matrix was computed from the inverse of the Hessian matrix. The standard error of estimates was computed from the variance-covariance matrix, which was used to quantify uncertainty in parameter estimates [53]. The standard error and mean estimate were used to calculate a 90% confidence regions for the parameter estimates. We suggest that larger the confidence region of an estimate, there is a higher uncertainty in the parameter estimate [53]. An optimal

parameter estimate is dependent on the minimization of SSE between prediction and data and the minimization of parameter uncertainty. The species parameters (τ, y_0, $y_{\max}$) were optimized separately across each of the three treatment conditions (GLU only, LPS only, GLU and LPS). The optimized reaction parameters (W, n, EC_{50}) stayed the same across the three treatment conditions as no significant difference in reaction parameters values was observed across these conditions. These optimized model parameters are provided in Section III A. It is relevant to note that the parameter optimization was carried out sequentially in the order of occurrence of species node in the network to avoid bias from multiple data points. For instance, ROS node gets activated prior to other response nodes in the network, hence tuning parameters for ROS activation was done independent of other data points in the data set.

As the curated biochemical data was obtained from multiple sources in our study, we normalized (Section II E), simulated, and trained the model to each data source separately. Additionally, we computed a 90% confidence region for the predictions by building a gaussian kernel density estimate around the mean and standard deviation or bandwidth of 0.05. We sampled 10000 points from the kernel density estimates, and obtained the quartiles to plot the 90% confidence region [54]. The trained model was able to capture the normalized levels of response variables such as IL-6, TNF-α, IL-1β, ROS, VEGF-A, eNOS, NO, p-Junction, and Gap Width. Furthermore, the predictions generated by the trained model for a short-term exposure to glucose and LPS were also validated by independent *in vitro* data sets that were not used in model training (Section III A).

E. Data Selection and Extraction

We curated data for our model by looking for experimental studies in published papers on Pubmed and Google Scholar. The data for model training and validation was selected from different studies based on the following criteria, (1) co-culture *in vitro* studies [13, 55] were used to study cell-cell interaction between macrophages and GECs with some exceptions [8, 9, 56, 57], (2) bone-marrow derived macrophages (BMDM) from diabetic subject and RAW 264.7 Murine macrophage cell line were most commonly considered [8, 9, 13, 57], (3) cells were stimulated with glucose concentration between 5 mM to 30 mM and LPS concentration between 0 $\mu g/ml$ to 0.1 $\mu g/ml$, and (4) protein concentration from bar graph or data tables at the end of each experiment at 6, 24, and 48 hours for three treatment conditions GLU only, LPS only, and GLU and LPS were available (Fig. 3). The co-culture experimental systems have gained interest in the field, especially for studying and engineering complex multi-cellular synthetic systems and mimicking tissue structures to some extent [58]. In absence of co-culture data, we extracted protein concentrations from individual cell culture studies done on either macrophages or endothelial cells [8, 9, 56, 57]. We extracted data from figures or tables in these publications [8, 9, 13, 55–57, 59–64] using WebPlotDigitizer, a web-based data extraction software [65]. In absence of quantified data, we used ImageJ software to quantify Western blot images from the published paper [66].

We normalized the curated data for two reasons, (1) to compare output from ODE-type LBM with data, and

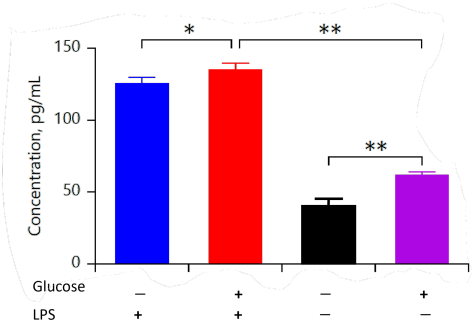

TR: GLU	TR: LPS	DA: TNFa	DV: TNFa	normalized
0	**0**	**0**	**45**	**0**
1	**0**	**0**	**45**	**0**
0	**1**	**0**	**45**	**0**
1	**1**	**0**	**45**	**0**
0	0	48	45	0
1	0	48	65	0.38
0	1	48	125	0.85
1	1	48	140	1

Sample MIDAS formatted csv file

FIG. 3. Sample bar graph (left) of protein concentration at different glucose or LPS treatment conditions as found in published studies. The mean values and upper bounds were obtained using Webplotdigizer. These values were stored in a MIDAS-formatted comma-separated values (csv) file in the following manner (right). TR:GLU and TR:LPS represents an active or inactive glucose and LPS treatment, respectively, where 0 represents inactive and 1 represents active treatment. DA: TNFa and DV:TNFa represents time (hours) and concentration (pg/ml) of a TNF-α protein, respectively. Normalized values in the table were obtained using method proposed in [24]. Baseline values (black bar) were used for each treatment condition at time 0 in the table (bold text). The values at 48 hours correspond to the respective treatment conditions in the bar graph. For instance, the data obtained from the blue bar corresponds to the highlighted row in the table.

(2) to pool data from multiple studies. It has been previously shown that it is important to normalize the data and simulations in the same way to ensure uniformity between model output and data [67]. Our model output lies between 0 and 1, thus we normalize the data in this range. Data normalization involves normalizing with respect to the highest value in the series, but this can overemphasize data outliers and underweight small and recurring differences in the series [24]. Instead, we used a multi-step non-linear data normalization technique in an open-source software, CellNOptR [68] proposed by Saez-Rodriguez *et al.* [24]. In order to perform data normalization in CellNOptR, the data was stored as a comma-separated values in a MIDAS-formatted file. Fig. 3 provides a concise representation of sample bar graphs, data table and structure, and normalized values. The data normalization was performed as follows, (1) normalized data between 0 and 1 by dividing each data value by the maximum value in the data series, (2) calculated relative change of each data point with respect to time 0, (3) transformed the relative change using a Hill function similar to (5), and (4) multiplied the transformed value and experimental noise (if any) to get the normalized data value. More detailed information on this normalization technique can be found in [24].

F. Model Assumptions

- Literature suggests a higher resolution of pro-inflammatory phenotype of macrophage cells during early stages of DKD [8]. We considered a pro-inflammatory phenotype of macrophages expressing pro-inflammatory species and ignored anti-inflammatory species for simplicity.

- GECs comprise a negatively charged matrix, the glycocalyx, which also contributes to endothelial permeability [3]. We focused on the glomerular endothelial cell layer only as we studied GEC signaling and dysfunction. However, glycocalyx signaling and characteristics are not part of this study.

- AGEs are mediators and drivers of diabetic complications [13, 69]. Our network assumed that glucose directly regulates AGE activation. The mechanism regulating glucose-dependent AGE activation is not part of this study.

- VEGFR-1 has 10-fold higher affinity for VEGF-A than VEGFR-2 does for VEGF-A. The tyrosine-kinase activity of VEGFR-1 is lower than VEGFR-2, which directly affects the signaling transduction process [34, 35]. We accounted for this 10-fold difference in receptor-ligand affinity and receptor kinase activity by tuning reaction weight W and half effect EC_{50} parameters, respectively [45]. Considering this difference in receptor activity in our network is a novel and relevant aspect of our model.

- The interaction kinetics across different endothelial cell lines are assumed to be same but protein levels of species may differ across cell lines [15]. This has been previously assumed in other models where data from different endothelial cell lines was curated in absence of studies on a specific cell line.

- Our protein signaling network considers only two types of cells, macrophages and GECs. These cells are stimulated by glucose and LPS, which mimics hyperglycemic and inflammatory response during early stages of DKD, respectively. We assume that full activation of glucose stimulus (i.e. $W_{GLU} = 1$) is analogous to a hyperglycemic range between 25-30 mM and full activation of LPS ($W_{LPS} = 1$) is same as an active LPS treatment in cultured cells (0.1 $\mu g/ml$). Using a fixed physiological range allowed us to extract protein expression data from different studies performed under similar treatment conditions.

G. Model Environment and Specifications

The model was developed with the help of multiple software packages supported in MATLAB and R. The ODEs were generated with the NetFlux package and solved using the ode23 function in MATLAB. The data normalization was done using the normaliseCNOlist in CellNOptR software package in R [70]. The model was simulated, fitted, and validated in MATLAB. The parameter estimation analysis, sensitivity, and uncertainty quantification was performed using the optimization toolbox in MATLAB [52]. The algorithm fmincon was used from the optimization toolbox to optimize model parameters and compute the Hessian matrix. We used the kde function to get kernel density estimates in MATLAB, which provide the confidence region around prediction mean [54].

III. RESULTS AND DISCUSSION

A. Model Training and Validation

The normalized-Hill differential equations logic-based modeling approach was applied to the macrophage and glomerular endothelial cell signaling network. The model was trained against normalized biochemical data for three separate treatment conditions, i.e. when only glucose stimulus is active (Fig. 4), when only LPS stimulus is active

(Fig. 5), or when both glucose and LPS stimuli are active (Fig. 6). The model was simulated for 48 hours based on the short-term analysis of co-culture systems in most published studies with a few exceptions. The intercellular response variables like IL-6, TNF-α, and IL-1β are fitted to co-culture data from macrophages and GECs. The intracellular response variables like ROS and VEGF-A in macrophage network were fitted to macrophage cell culture data, whereas variables like ROS$_{ec}$, eNOS, and NO in GECs were fitted to endothelial cell culture data.

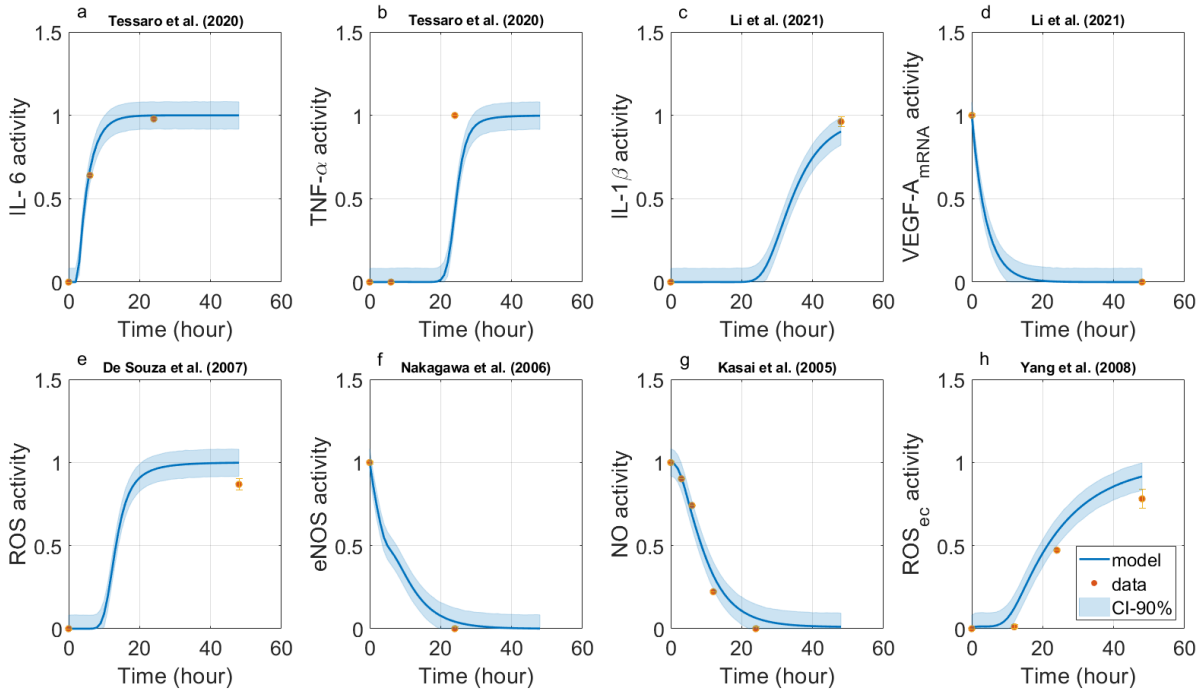

FIG. 4. Network model trained to biochemical data from [9, 13, 56, 57, 59, 61] upon stimulation with glucose only for 48 hours (W_{GLU}=1, W_{LPS}=0). This is a semi-quantitative comparison of model response against normalized protein levels of IL-6 (a), TNF-α (b), IL-1β (c), VEGF-A (mRNA) levels (d), ROS fluorescence (e), nitric oxide (NO) (g), eNOS (f), and ROS in glomerular endothelial cells (h). Blue curves are model predictions, orange points are data points, and blue shaded region is 90% confidence region. Species activity above half maximal activity (0.5) denote relative upregulation, and species activity below half maximal activity (0.5) denote relative downregulation. The subscript "ec" denotes intracellular expression in glomerular endothelial cells.

The model was simulated with *GLU* treatment, where glucose stimulus was active and LPS stimulus was inactive. We observed that *GLU* treatment significantly upregulated pro-inflammatory cytokine IL-6 as early as 6 hours of treatment (Fig. 4 (b)). Cytokines such as TNF-α and IL-1β were upregulated after 24 hours in presence of glucose (Fig. 4 (a) and (c)). This upregulation of pro-inflammatory cytokines can further augment the phenotypic switch towards the pro-inflammatory state in macrophages in the early stage of DKD. *GLU* treatment significantly downregulated VEGF-A secretion by macrophages (Fig. 4 (d)). On the contrary, studies performed in diabetic subjects showed a systemic upregulation of VEGF levels. Our observations suggest that another stimulus and regulatory species may be involved besides glucose. Moreover, macrophages are the only source of VEGF-A secretion in our model, which could explain this contradictory observation. The downregulation of VEGF-A activity caused downregulation of eNOS and reduction in NO bioavailability in GECs (Fig. 4 (f), (g)). Although our network model considers a simplified

VEGF-dependent eNOS/NO pathway, it is still able to predict glucose-mediated NO downregulation. Based on model predictions and literature evidence, glucose stimulation alone can significantly upregulate ROS activity in both macrophages and GEC, Fig. 4 (e), (h). In GECs, the uncoupling of eNOS from its pathway triggered an over-expression of ROS_{ec} as by-product. This upregulation of ROS_{ec} is correlated with the simultaneous downregulation of NO and upregulation of ONOO in our model. In macrophages, ROS was upregulated due to glucose-mediated upregulation of AGEs and NADPH.

The model was stimulated with LPS treatment, where LPS stimulus was active and glucose stimulus was inactive (Fig. 5). LPS stimulus is a pro-inflammatory stimulus that upregulates inflammatory cytokines like IL-6, TNF-α, and IL-1β in our network. The activity of IL-6, TNF-α, and IL-1β increased 6 hours after activation by LPS stimulus in our network (Fig. 5 (a), (b), (c)). This observation is different from GLU treatment shown above as LPS is a pro-inflammatory stimulus and more potent regulator of pro-inflammatory cytokines. We observed that LPS stimulus alone upregulated VEGF-A activity in macrophages via PI3K-Akt and NFκB pathway in our network. The upregulated VEGF-A activates VEGF receptors on GECs (Fig. 5 (d)). As mentioned earlier, VEGF-A protein can initiate downstream signaling through competitive binding to its receptors (VEGFR-1, VEGFR-2). The VEGFR-1 and VEGFR-2 receptor affinity to VEGF-A was estimated by changing W and EC_{50} parameters. The species and reaction parameters for VEGF receptors were estimated by simulating LPS-dependent VEGF-A activation of endothelial cells. The results from these model simulations are given in Appendix (Fig. A1). These optimized W and EC_{50} parameter values can be found in Table I. Further, VEGF-A upregulation caused increased eNOS and NO activity (Fig. 5 (f), (g)). ROS expression was upregulated due to PI3K-dependent pathway in macrophages (Fig. 5 (e)) and eNOS-dependent pathway in GECs (Fig. 5 (h))

Upon stimulation with both glucose and LPS stimuli, the network model predicts a synergic response when both stimuli were active as shown in Fig. 6. We calibrated the model responses such as IL-6, TNF-α, IL-1β, ROS, VEGF-A, eNOS, NO, and ROS_{ec} for this treatment condition. We observed that pro-inflammatory cytokines (Fig. 6 (a), (b), (c)) and ROS (Fig. 6 (e), (h)) were upregulated as also seen for other treatment conditions. VEGF-A activity was increased in macrophages after an initial delay which is possibly due to a combination of glucose-dependent downregulation and LPS-dependent upregulation of VEGF-A (Fig. 6 (d)). Similarly, we observed that NO activity was upregulated with a slight delay, which shows the negative effect of glucose on NO and the positive effect of LPS and VEGF on NO (Fig. 6 (g)). In our network, when both glucose and LPS stimuli were active, LPS stimulus dominated the expression of growth factors, cytokines, and ROS.

The optimized species and reaction parameters are provided in Table I and II. The most sensitive reaction weight parameters (W) were optimized, rest were set to default value of 1. Reaction weight value of 1 implies that 100% of input is available for 100% activation or inhibition of output species. Similarly, sensitive half effect (EC_{50}) parameters were optimized, rest were set to default value of 0.5. Any value below 1 suggests less than 100% activation or inhibition of output species. EC_{50} value below or above 0.5 suggests that less than 50% or more than 50% of input species is required to achieve maximum output activity, respectively. The initial value (y_0) has a default value of 0. For

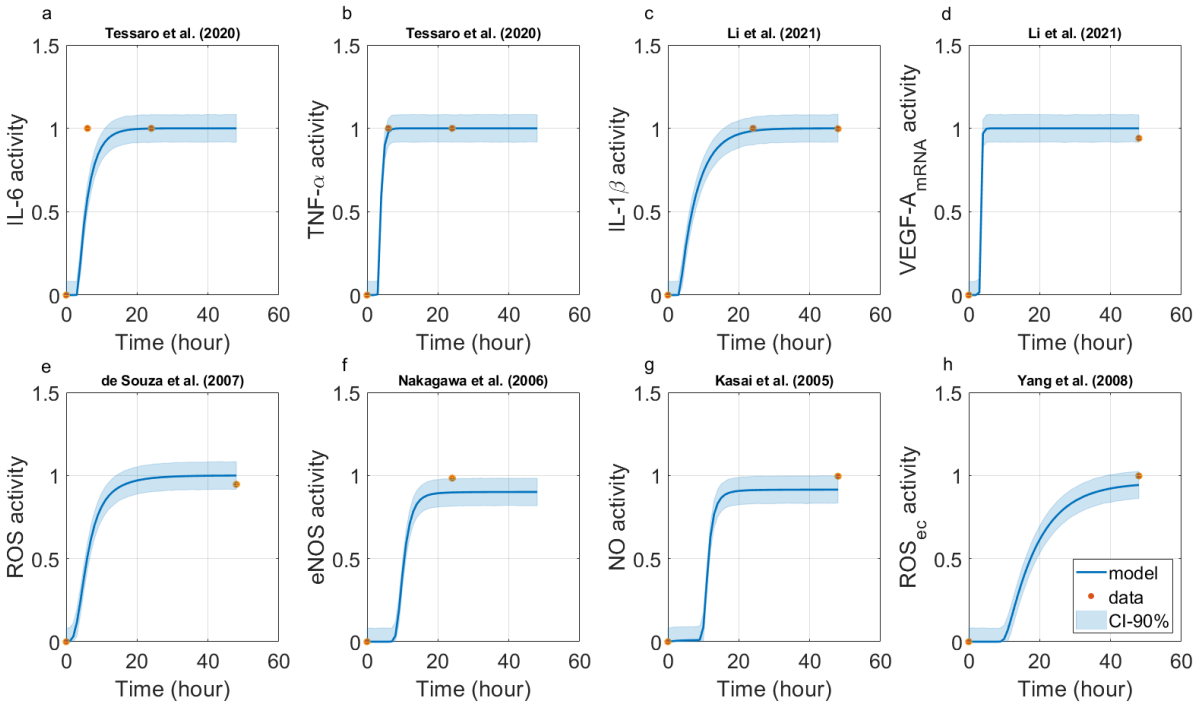

FIG. 5. Network model trained to biochemical data from [9, 13, 56, 57, 59, 61] upon stimulation with LPS only for 48 hours (W_{GLU}=0, W_{LPS}=1). This is a semi-quantitative comparison of model response against normalized protein levels of IL-6 (a), TNF-α (b), IL-1β (c), VEGF-A (mRNA) levels (d), ROS fluorescence (e), nitric oxide (NO) (g), eNOS (f), and ROS in glomerular endothelial cells (h). Blue curves are model predictions, orange points are data points, and blue shaded region is 90% confidence region. Species activity above half maximal activity (0.5) denote relative upregulation, and species activity below half maximal activity (0.5) denote relative downregulation. The subscript "ec" denotes intracellular expression in glomerular endothelial cells.

VEGF-A (mRNA), NO, eNOS, and VEGF-A species, the initial value was estimated close to 1 in order to capture the downregulation effect in *GLU* only treatment (Table II).

The trained model is validated with available *in vitro* validation dataset from multiple sources [8, 60–64, 71] that are not part of the training dataset. The model validation is performed across three treatment conditions, *GLU* (Fig. 7), *LPS* (Fig. 8), and *GLU* and *LPS* (Fig. 9). The trained model simulations agree with available validation data for TNF-α, IL-6, IL-1β, ROS, VEGF-A, eNOS, NO,and ROS$_{ec}$. In Fig. 7 (c), IL-1β activity could not be validated by validation data due to lack of sufficient training data for different simulation time points. In addition, we also validated other regulatory species in the network that were not fitted during model training. These species include phosphorylated VE-Cadherin activity (Fig. 8 (e)), calcium (Ca) activity, and glomerular endothelial fenestration ($GapWidth$) (Fig. A2). The change in endothelial fenestration width denotes change in gap width between intercellular GECs from baseline. The gap width in our network is modulated directly by phosphorylation of cell-cell junction proteins such as VE-Cadherin, which is responsible for the opening of these cell-cell junctions. There are limited published studies that report glomerular endothelial fenestration width in diabetic state. However, we were able to qualitatively show the effect of high glucose levels and dysregulated signaling on fenestration width. These short-term model simulations contribute to our understanding of dysregulated signaling interactions between

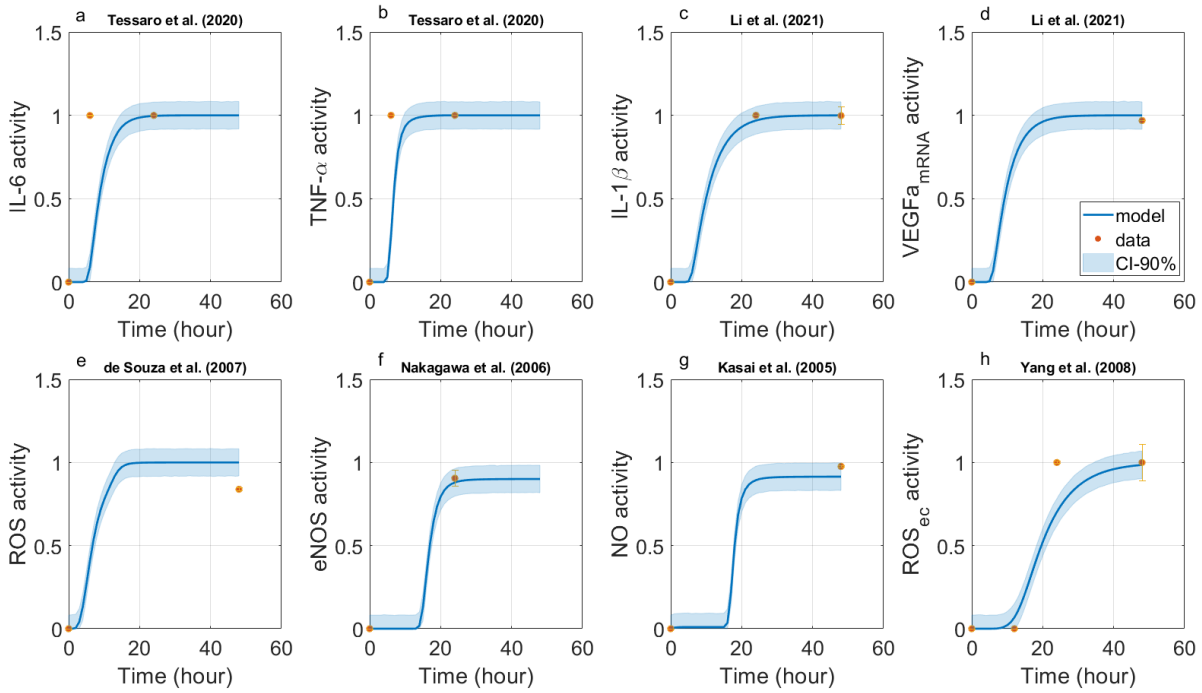

FIG. 6. Network model trained to biochemical data from [9, 13, 56, 57, 59, 61] upon stimulation with glucose and LPS for 48 hours (W_{GLU}=1, W_{LPS}=1). This is a semi-quantitative comparison of model response against normalized protein levels of IL-6 (a), TNF-α (b), IL-1β (c), VEGF-A (mRNA) levels (d), ROS fluorescence (e), nitric oxide (NO) (g), eNOS (f), and ROS in glomerular endothelial cells (h). Blue curves are model predictions, orange points are data points, and blue shaded region is 90% confidence region. Species activity above half maximal activity (0.5) denote relative upregulation, and species activity below half maximal activity (0.5) denote relative downregulation. The subscript "ec" denotes intracellular expression in glomerular endothelial cells.

macrophages and GECs. Despite a short-term exposure of 48 hours to glucose and LPS, these cells undergo significant perturbations in signaling pathways and molecules. Therefore it is essential to study dysregulated signaling pathways not just *in vitro* but also *in vivo*. A deeper understanding of signaling dysregulation in the early stage of DKD can guide us to a mechanistic link between diabetes-mediated immune response and cellular dysfunction in GECs.

B. Analysis of Protein Signaling Network

Through our network, we demonstrated the effect of hyperglycemia on cell signaling pathways, cellular microenvironment, and resulting perturbations in both macrophages and GECs. We demonstrated that significantly high levels of glucose and LPS affect macrophage phenotype and activate GECs. The model captured this change in phenotype in macrophages with an increased expression of pro-inflammatory species such as IL-6, TNF-α, IL-1β, and ROS by both macrophages and GECs. These pro-inflammatory species affects macrophage phenotype through autocrine or paracrine signaling [72]. The consistent secretion of these inflammatory molecules and ongoing inflammation lead to a chronic shift of macrophage phenotype [72]. Although not all such autocrine or paracrine signaling interactions were included in our network, we depicted this effect on macrophages through ROS-mediated PI3K signaling and VEGF-

TABLE I. List of reaction parameters for the model. Reaction weight (W), Hill coefficient (n), and half maximal effect (EC_{50}) are shown for respective reaction rules or interactions. Reaction rule $A\&B => C$ denotes an AND logic operator between input A and input B to give output C. Reaction rule $A => C$ denotes input A gives output C. Default values of W, n, EC_{50} are 1, 1.4, and 0.5, respectively.

Reaction Rule	W	n	EC_{50}
$=> GLU$	0	3.149	0.5
$=> LPS$	0	3.266	0.5
$LPS => TLR4$	1	3.556	0.5
$GLU => AGE$	1	4.290	0.5
$AGE => RAGE$	1	3.284	0.5
$RAGE => NADPH$	1	4.846	0.5
$TLR4 \ \& \ ROS => NFKB$	1	4.789	0.112
$TLR4 => PI3K$	1	3.789	0.002
$NADPH => ROS$	1	4.771	0.5
$PI3K => AKT$	1	4.508	0.5
$PI3K => ROS$	1	3.262	0.5
$NFKB_{ec} => TNF\alpha$	1	4.007	0.25
$AKT => NFKB$	1	4.129	0.5
$NFKB => IL6$	1	4.539	0.5
$NFKB = TNF\alpha$	1	4.290	0.5
$NFKB => VEGFa_{mRNA}$	1	4.959	0.5
$VEGFa_{mRNA} => VEGFa$	1	4.391	0.5
$NFKB => IL1\beta$	1	4.786	0.5
$VEGFa => VEGFR_1$	1	2.821	0.5
$VEGFa => VEGFR_2$	0.727	3.11	0.5
$AGE => RAGE_{ec}$	1	3.164	0.5
$RAGE_{ec} => NADPH_{ec}$	1	4.585	0.5
$VEGFR_2 => PI3K_{ec}$	1	4.435	0.5
$VEGFR_1 => PI3K_{ec}$	0.9	4.828	0.5
$NADPH_{ec} => ROS_{ec}$	1	4.370	0.989
$PI3K_{ec} => AKT_{ec}$	0.5	4.898	0.5
$AKT_{ec} => eNOS$	0.906	3.188	0.103
$VEGFR_1 => PLC\gamma$	1	3.536	0.5
$PLC\gamma => NFKB_{ec}$	1	3.572	0.5
$ROS_{ec} => NFKB_{ec}$	1	4.851	0.5
$NFKB_{ec} => IL6$	1	4.264	0.003
$NFKB_{ec} => IL1\beta$	1	3.523	0.5
$eNOS => NO$	0.989	4.954	0.638
$eNOS => ROS_{ec}$	1	3.375	0.989
$ROS_{ec} \ \& \ NO => ONOO$	1	4.007	0.5
$!NO => Ca$	1	2.542	0.5
$PLC => Ca$	1	2.827	0.5
$Ca => pJunction$	1	2.605	0.5
$pJunction => GapWidth$	1	3.18	0.5
$Ca => NO$	0.01	1.4	0.5

mediated VEGF receptor activation. In our network (Fig. 1), an over-expression of intracellular ROS activity in the

TABLE II. List of species parameters for the model species. Optimized time constant (τ) and initial value (y_0) for respective species are shown for each treatment condition. "-" indicates that parameter values were set to default. Default values of τ and y_0 are 1 hour and 0, respectively.

	GLU only		*LPS* only	*GLU* and *LPS*
Species	τ	y_0	τ	τ
GLU	0.024	–	–	3.019
LPS	–	–	4.695	3.003
$VEGFa_{mRNA}$	4.085	0.998	0.054	4.005
$RAGE$	7.57	–	–	10
$NADPH$	7.97	–	7.733	3.016
$NFKB$	–	–	–	2.985
NO	6.89	1	0.055	0.0548
$eNOS$	6.568	1	1.471	1.745
$VEGFa$		0.998	–	–
ROS_{ec}	15	–	–	8
$pJunction$	0.014	–	2.549	–
Ca	–	–	2.974	–
$GapWidth$	–	–	2.230	–

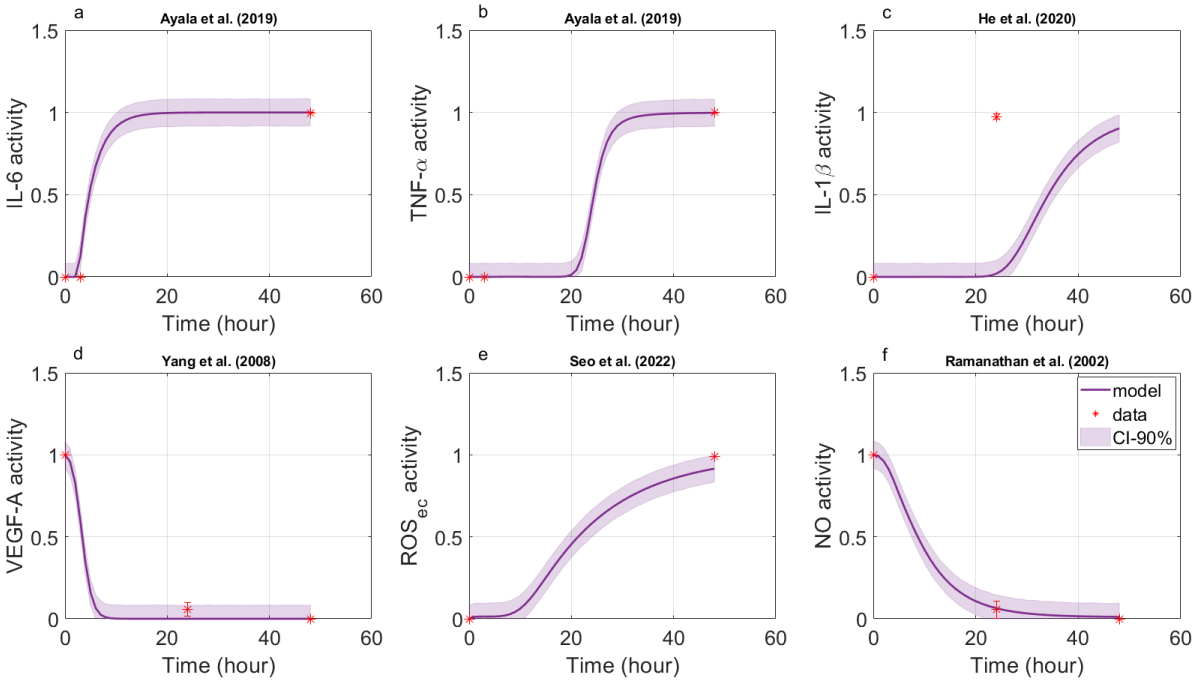

FIG. 7. Network responses are validated with biochemical data available from cell culture experiments [8, 60–63] upon stimulation with high glucose for 48 hours (W_{GLU}=1, W_{LPS}=0). Model validation of selected species against available normalized protein levels of IL-6 (a), TNF-α (b), IL-1β (c) protein levels, VEGF-A levels (d), ROS in glomerular endothelial cells (e), and nitric oxide (NO) (f). Purple curves are model predictions, orange points are validation data points, purple shaded region is 90% confidence region. Species activity above half maximal activity (0.5) denote relative upregulation, and species activity below half maximal activity (0.5) denote relative downregulation. The subscript "ec" denotes intracellular expression in glomerular endothelial cells.

macrophages is preliminary to causing disturbance to downstream signaling (Fig. 4 (e), 5 (e)). As ROS is activated

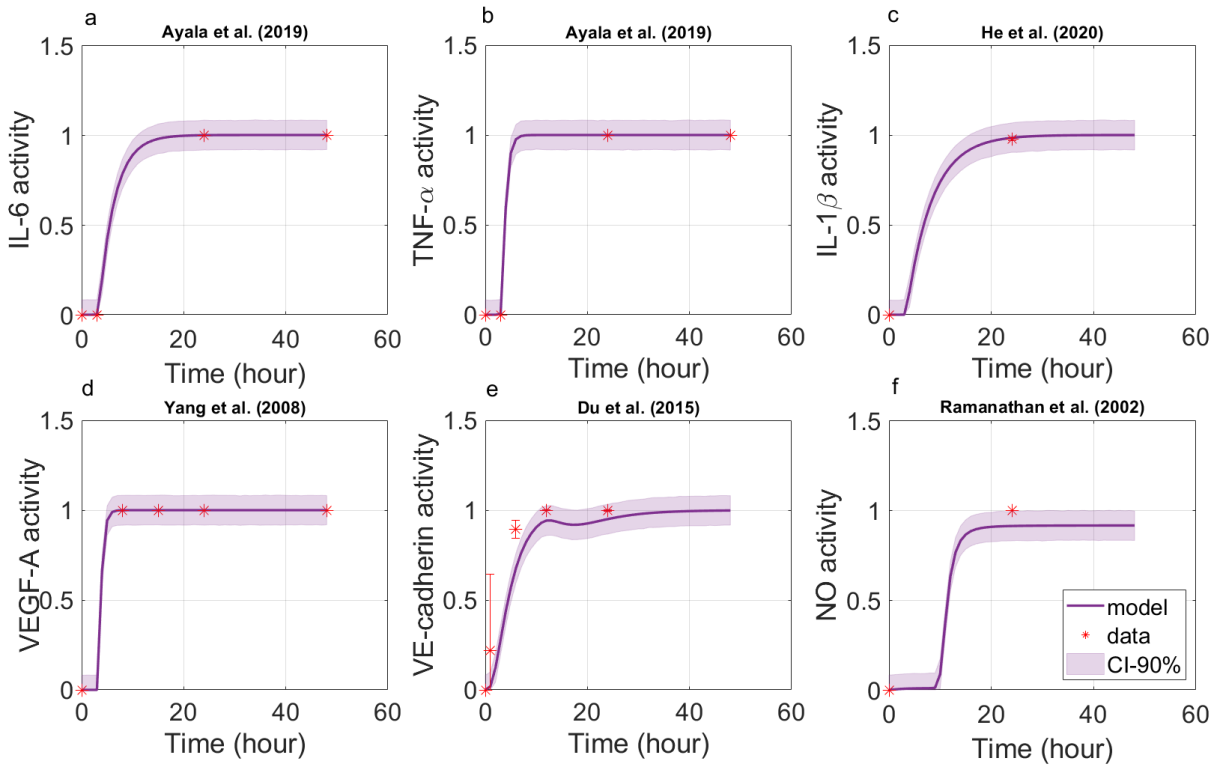

FIG. 8. Network responses are validated with biochemical data available from cell culture experiments [8, 60, 61, 63, 64] upon stimulation with LPS for 48 hours (W_{GLU}=0, W_{LPS}=1). Model validation of selected species against available normalized protein levels of IL-6 (a), TNF-α (b), IL-1β (c) protein levels, VEGF-A levels (d), phosphorylated VE-cadherin (e), and nitric oxide (NO) (f). Purple curves are model predictions, orange points are validation data points, purple shaded region is 90% confidence region. The subscript "ec" denotes intracellular expression in glomerular endothelial cells.

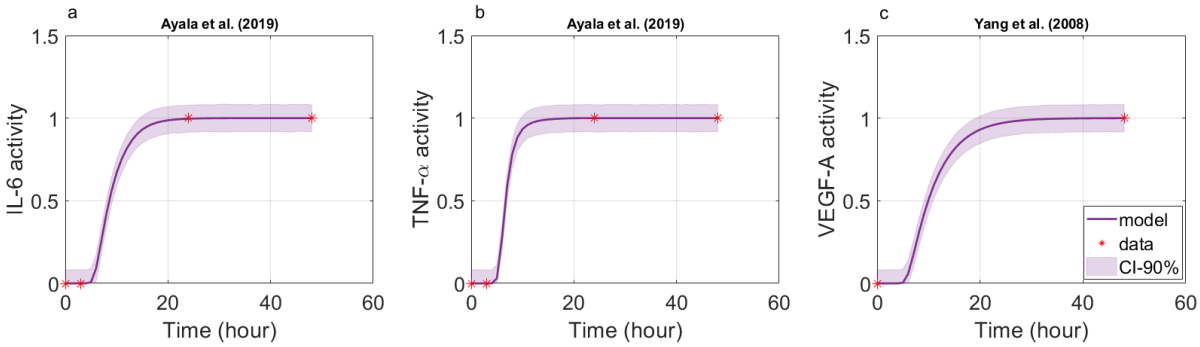

FIG. 9. Network responses are validated with biochemical data available from cell culture experiments [8, 61] upon stimulation with glucose and LPS for 48 hours (W_{GLU}=1, W_{LPS}=1). Model validation of selected species against available normalized protein levels of IL-6 (a), TNF-α (b), and VEGF-A (c). Purple curves are model predictions, orange points are validation data points, purple shaded region is 90% confidence region.

via multiple routes by either stimulus, it is a relevant link that should be explored in order to target dysregulated downstream pathways.

Co-culture experimental studies showed that elevated glucose levels without a pro-inflammatory stimulus cannot significantly upregulate cytokine or VEGF-A expression [13]. In our network, an AND logical rule between LPS-

stimulated PI3K signaling and glucose-stimulated ROS signaling ensured that pro-inflammatory species cannot be activated without LPS. Active VEGF-A selectively binds to its receptors VEGFR-1 and VEGFR-2 on GECs with different affinities. We estimated that the reaction weight for VEGFR-2 activation by VEGF-A is less than 1, which confirms that VEGF-A has less affinity for VEGFR-2 than VEGFR-1. We also estimated that the reaction weight for activation of $PI3K_{ec}$ by VEGFR-1 is less than 1, which confirms that VEGFR-1 has a relatively lower kinase activity than VEGFR-2. The lower kinase activity of VEGFR-1 and its higher affinity to VEGF-A affects its downstream response to PI3K-Akt kinases. VEGFR-1 also promotes downstream pro-inflammatory signaling via PLC-γ/PKC pathway. As a result of this biased affinity to VEGF-A, the cellular response and behavior of the activated GECs was affected. The resulting perturbations involved insufficient activation of VEGF-mediated PI3K-Akt signaling, reduced NO bioavailability due to uncoupling of endothelial NO, increased pro-inflammatory cytokines expression, and macrophage infiltration. These observations suggest that targeting this competitive receptor activation by VEGF-A could be useful in modulating signaling dysregulation in GECs.

Our model showed the effect of VEGF-dependent signaling and NO bioavailability on junction protein phosphorylation. From a molecular standpoint, the endothelial barrier is sealed by cell-cell junction proteins, among which VE-cadherin serves as a cornerstone. The endothelial barrier is maintained by VE-cadherin and associated catenins in a non-phosphorylated state [48]. The modulated phosphorylation of these junction proteins allows for selective opening or closing of the barrier. The relationship between VEGF-dependent NO and phosphorylated junction proteins was captured as a negative feedback loop in the network. The use of negative feedback loop between NO and calcium allowed for better information processing and cell behavior regulation in our network. Lower than normal NO levels in GECs affected barrier integrity reversibly [26]. We showed that hyperglycemic conditions caused a prolonged and consistent disruption of the GEC barrier integrity. Ultimately, this reduced cell-cell junction integrity widens the intercellular gaps between GECs. Therefore, it is relevant to target this mechanistic pathway that links NO and GEC junction integrity to mitigate glomerular endothelial dysfunction.

The validated network model can be used to make insightful predictions under different combinations of stimuli treatments. The model simulations shown previously were performed in presence of full activation of each stimulus. We also predicted network responses under partial activation of either stimulus. We varied the reaction weight (W) for glucose and LPS stimulus to study the potency of either stimulus. Fig. 10 shows the predicted response under varying glucose activity and no LPS stimulus. In Fig. 10 (a), we observed that less than a quarter of maximum glucose activity ($W_{GLU} < 0.25$) was sufficient to activate and express IL-6 cytokine. However, this low glucose activity is not sufficient to sustain IL-6 expression after 24 hours, after which IL-6 activity returns to baseline level. Intracellular ROS was expressed in macrophages when stimulated with low glucose levels below 0.25 (Fig. 10 (b)). We observed reduced expression of PLC-γ protein in presence of low glucose levels and absence of LPS stimulus (Fig. 10 (c)). As previously observed, glucose stimulus downregulated VEGF-A activity, which could be the reason for the lowered PLC-γ activity in Fig. 10 (c). We observed that gap width between GECs was not restored by simply reducing glucose levels to baseline (Fig. 10 (d)), and further analysis is needed to identify signaling interactions responsible

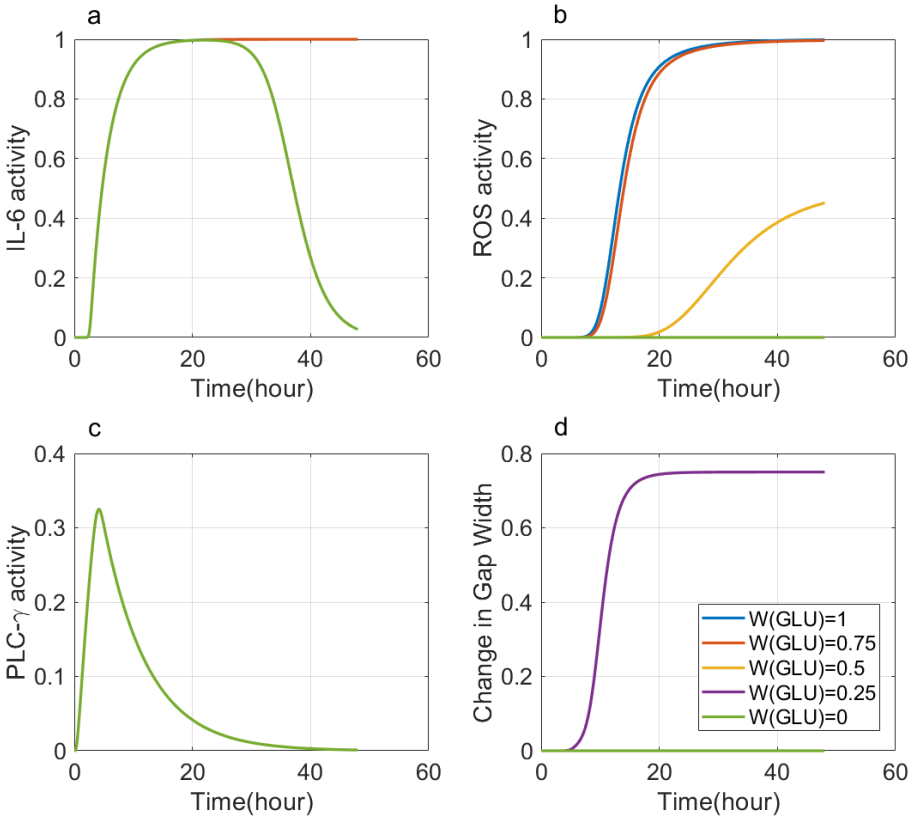

FIG. 10. Model predictions upon stimulation with partially active GLU stimulus to mimic the increase in glucose levels in the early stage of diabetes. W_{GLU} varied between 0 to 1. W_{LPS} is set to 0 to mimic a non-inflammatory state. The above prediction is qualitative and suggests the change in protein expression from baseline.

for gap width change in GECs. Fig. 11 shows predicted response when LPS activity was varied under high glucose levels. This scenario mimics the early phase of DKD development, where poor glycemic control and high glucose levels can be observed with gradual increase in pro-inflammatory species and environment. Increasing levels of LPS activity had a strong effect on over-expression of pro-inflammatory cytokine, TNF-α (Fig. 11 (a)). PLC-γ protein was upregulated in presence of partial LPS activity, Fig. 11 (c). We observed that downregulated NO levels slowly recovered to baseline levels as normalized LPS activity increased from 0 to 1 (Fig. 11 (d)). A minimum LPS activity of 0.25 was sufficient to recover downregulated NO levels. LPS stimulus regulates VEGF-A expression in macrophages, which is responsible for restoring NO levels to baseline.

These model prediction demonstrated the potency of both input stimuli on the network response and behavior, and respective threshold activity of glucose and LPS to initiate short-term pro-inflammatory response. However, we are interested in identifying influential pathways from our network model, which trigger inflammation, and GEC activation and dysfunction in the early stage of DKD. We performed a local sensitivity analysis on the validated model using methods described previously. The effect of infinitesimal perturbations in reaction weight (W), half effect (EC_{50}), and time constant (τ) parameters was observed on model responses. Reaction weight and half effect parameter have biological relevance when determining the interaction between species. Time constant parameter regulates the overall

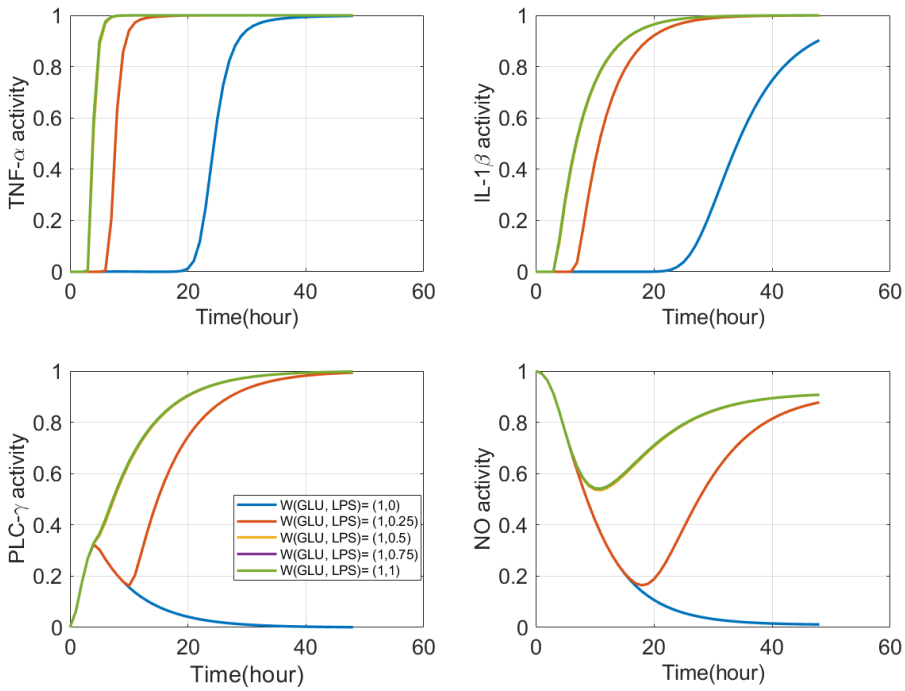

FIG. 11. Model predictions upon stimulation with partially active LPS and fully active GLU stimulus ($W_{GLU} = 1$) to mimic gradual rise in inflammation in early stage of DKD. W_{LPS} varied between 0 and 1. The above prediction is qualitative and suggests the change in protein expression from baseline. The choice of initial values (0 or 1) were subject to upregulation or downregulation from baseline values (at healthy state).

rate of a species in the network. The parameter sensitivity was computed with respect to change in the species output at 48 hours. The heatmap of τ parameter sensitivity suggests a strong positive effect of τ_{NO} parameter on NO and TNF-α expression at 48 hours (Fig. A6). However, τ_{NO} had a negative effect on GEC gap width, which is due to the negative feedback loop between NO and calcium. Moreover, τ_{AGE}, $\tau_{VEGFRec1}$, τ_{ROS}, τ_{TNFa}, and τ_{VEGFa} also affected TNF-α and GEC gap width to some degree. Fig. A7 suggests that W_{40} parameter corresponding to $Ca = NO$ interaction was the most influential interaction in the network. EC_{50} parameters corresponding to $TLR4 = PI3K$ and $NFkBec = IL6$ directly affected TNF-α activity, and inversely affected NO activity and GEC gap width (Fig. A8). These identified interactions can be further analysed individually through experiments. Together, our predictive findings indicate that a multi-targeted approach is necessary to modulate the early markers of DKD.

IV. CONCLUSIONS

In this study, we presented a multi-cell logic-based ODE model to understand the role of diabetes and immune response in the progression of microvascular complications in the diabetic kidney. We created a signaling network of crosstalk between macrophages and GECs stimulated by two inputs, high glucose, and LPS, a pro-inflammatory stimulus. The signaling network was modeled using continuous ODEs and logic-based interaction rules, where interaction between species was formulated using normalized-Hill functions. The model was trained and validated against

published data from *in vitro* experiments performed on murine macrophage cell lines and endothelial cell lines. Our modeling approach combines the advantages of quantitative biochemical models and qualitative LBMs. These pathways and interactions between macrophages and GECs in the early stage of DKD have not been computationally studied before. Our model also incorporated the effect of competitive activation of VEGF receptors in activated GECs, which is less understood. We validated the signaling interactions and model responses against published data for short-term exposure to either stimulus. In presence of high glucose and a pro-inflammatory stimulus like LPS, we observed upregulation of normalized protein values of pro-inflammatory cytokines (IL-6, TNF-α, and IL-1β), oxidative stress, VEGF-A, and GEC fenestration width. We found that oxidative stress in macrophages significantly affected interconnected downstream species, pathways, NF-κB transcription factor, and NO bioavailability. Through our signaling network, we have studied glucose-mediated inflammatory pathways in the diabetic kidney, which can contribute to a comprehensive understanding of DKD development and progression. We addressed the gap in knowledge on mechanisms and interactions responsible for macrophage-dependent inflammation and glomerular endothelial dysfunction in the early stage of DKD. Our results contribute to the understanding of signaling and molecular perturbations on GEC morphology. Moreover, our network and model findings can be leveraged to scale up from *in vitro* to *in vivo* data.

V. ACKNOWLEDGEMENT

This work was supported by National Institutes of Health grant R35GM133763, National Science Foundation grant 2133411, and the University at Buffalo. We would like to thank lab members for their thorough feedback on this manuscript.

REFERENCES

[1] Centers for Disease Control and Prevention. National Diabetes Statistics Report, 2020. `https://www.cdc.gov/diabetes/data/statistics-report/index.html`.

[2] S. Thomas and J. Karalliedde. Diabetic kidney disease. Medicine, 50:704–710, 2022.

[3] J. Yang and Z. Liu. Mechanistic pathogenesis of endothelial dysfunction in diabetic nephropathy and retinopathy. Frontiers in Endocrinology, 13:816400, 2022.

[4] H. Thomas and A. Ford Versypt. Collagen deposition in diabetic kidney disease boosts intercellular signaling: A mathematical model. bioRxiv, 2021.

[5] H. Thomas and A. Ford Versypt. Pathophysiology of mesangial expansion in diabetic nephropathy: mesangial structure, glomerular biomechanics, and biochemical signaling and regulation. J Biol Eng, 16, 2022.

[6] J. F. Navarro-González, C. Mora-Fernández, M. Muros de Fuentes, and J. García-Pérez. Inflammatory molecules and pathways in the pathogenesis of diabetic nephropathy. Nat Rev Nephrol., 7:327–40, 2011.

[7] S. Tsalamandris, A. S. Antonopoulos, E. Oikonomou, G. A. Papamikroulis, G. Vogiatzi, S. Papaioannou, S. Deftereos, and D. Tousoulis. The role of inflammation in diabetes: Current concepts and future perspectives. Eur. Cardiol., 14:50–59, 2019.

[8] T. S. Ayala, F. H. G. Tessaro, G. P. Jannuzzi, L. M. Bella, K. S. Ferreira, and J. O. Martins. High glucose environments interfere with bone marrow-derived macrophage inflammatory mediator release, the TLR4 pathway and glucose metabolism. Sci. Rep., 9, 2019.

[9] F. H. Galvão Tessaro, T. S. Ayala, L. M. Bella, and J. O. Martins. Macrophages from a type 1 diabetes mouse model present dysregulated PI3K/AKT, ERK 1/2 and SAPK/JNK levels. Immunobiology, 225, 2019.

[10] S. Rayego-Mateos, J. Morgado-Pascual, L. Opazo-Rios, M. Guerrero-Hue, C. García-Caballero, C. Vázquez-Carballo, S. Mas, B. Sanz, C. Herencia, S. Mezzano, C. Gomez-Guerrero, J. Moreno, and J. Egido. Pathogenic pathways and therapeutic approaches targeting inflammation in diabetic nephropathy. Int. J. Mol. Sci., 21:3798, 2020.

[11] R. Z. Alicic, M. T. Rooney, and K. R. Tuttle. Diabetic kidney disease: Challenges, progress, and possibilities. Clin. J. Am. Soc. Nephrol., 12, 2017.

[12] C. Johnson-Léger and B. Imhof. Forging the endothelium during inflammation: Pushing at a half-open door? Cell Tissue Res., 314:93–105, 2003.

[13] Y. Li, W. Yu, M. He, and F. Yuan. The effects of m1/m2 macrophages on the mrna expression profile of diabetic glomerular endothelial cells. Nephron, 145:1–11, 2021.

[14] T. Takahashi and R. C. Harris. Role of endothelial nitric oxide synthase in diabetic nephropathy: Lessons from diabetic enos knockout mice. J. Diabetes Res., 2014:590541, 2014.

[15] Q. Wu and S. Finley. Mathematical model predicts effective strategies to inhibit VEGF-eNOS signaling. J. Clin. Med., 9:1255, 2020.

[16] H. J. Zhao, S. Wang, H. Cheng, M. Z. Zhang, T. Takahashi, A. B. Fogo, M. D. Breyer, and R. C. Harris. Endothelial nitric oxide synthase deficiency produces accelerated nephropathy in diabetic mice. J. Am. Soc. Nephrol., 17:2664–9, 2006.

[17] A. Shu, Q. Du, J. Chen, Y. Gao, Y. Zhu, G. Lv, J. Lu, Y. Chen, and H. Xu. Catalpol ameliorates endothelial dysfunction and inflammation in diabetic nephropathy via suppression of RAGE/RhoA/ROCK signaling pathway. Chem.-Biol. Interact., 348:109625, 2021.

[18] D. O. Bates. Vascular endothelial growth factors and vascular permeability. Cardiovasc. Res., 87:262–271, 2010.

[19] S. Satchell and J. Tooke. What is the mechanism of microalbuminuria in diabetes: A role for the glomerular endothelium? Diabetologia, 51:714–25, 2008.

[20] W. Deen, M. Lazzara, and B. Myers. Structural determinants of glomerular permeability. Am. J. Physiol.: Renal Physiol., 281:F579–96, 2001.

[21] T. H. Hostetter, E. B. Hauser, B. S. Daniels, and W. M. Deen. Glomerular basement membrane: In vitro studies of water and protein permeability. Am J Physiol., 262:F919–26, 1992.

[22] P. Dechadilok and W. M. Deen. Hindrance factors for diffusion and convection in pores. Ind. Eng. Chem. Res., 45, 2006.

[23] D. A. Lorenzo, M. I. Lin, T. Murata, S. Landskroner-Eiger, M. Schleicher, M. Kothiya, Y. Iwakiri, J. Yu, P. Huang, and W. Sessa. eNOS-derived nitric oxide regulates endothelial barrier function through VE-cadherin and Rho GTPases. J. Cell Sci., 127:2120, 2014.

[24] J. Saez-Rodriguez, L. G. Alexopoulos, J. Epperlein, R. Samaga, D. A. Lauffenburger, S. Klamt, and P. K. Sorger. Discrete logic modelling as a means to link protein signalling networks with functional analysis of mammalian signal transduction. Mol. Syst. Biol., 5:331, 2009.

[25] M. J. Kraeutler, A. R. Soltis, and J. J. Saucerman. Modeling cardiac -adrenergic signaling with normalized-hill differential equations: Comparison with a biochemical model. BMC Syst. Biol., 4:157, 2010.

[26] N. Weinstein, L Mendoza, I. Gitler, and J. Klapp. A network model to explore the effect of the micro-environment on endothelial cell behavior during angiogenesis. Front. Physiol., 8, 2017.

[27] J. Saez-Rodriguez, L. Simeoni, J. A. Lindquist, R. Hemenway, U. Bommhardt, B. Arndt, U. U. Haus, R. Weismantel, E. D. Gilles, S. Klamt, and B. Schraven. A logical model provides insights into T cell receptor signaling. PLoS computational biology, 3:e163, 2007.

[28] J. Fu, K. Akat, Z. Sun, W. Zhang, D. Schlondorff, H. Liu, T. Tuschl, K. Lee, and J. He. Single-cell RNA profiling of glomerular cells shows dynamic changes in experimental diabetic kidney disease. J. Am. Soc. Nephrol., 30:533–545, 2019.

[29] M. Kanehisa and S. Goto. Kegg: kyoto encyclopedia of genes and genomes. Nucleic Acids Res., 28:27–30, 2000.

[30] A. R. Pico, T. Kelder, van Iersel M. P., K. Hanspers, B. R. Conklin, and Evelo C. Wikipathways: Pathway editing for the people. PLOS Biology, 6:1–4, 2008.

[31] I Afanasév. Signaling of reactive oxygen and nitrogen species in diabetes mellitus. Oxid. Med. Cell. Longevity, 3:361–373, 2010.

[32] E. Rendra, V. Riabov, D. M. Mossel, T. Sevastyanova, M. C. Harmsen, and J. Kzhyshkowska. Reactive oxygen species (ROS) in macrophage activation and function in diabetes. Immunobiology, 224, 2018.

[33] W. Durán, J. Breslin, and F. Sanchez. The NO cascade, eNOS location, and microvascular permeability. Cardiovasc. Res., 87:254–61, 2010.

[34] M. Shibuya. Vascular endothelial growth factor receptor-1 (VEGFR-1/Flt-1): A dual regulator for angiogenesis. Angiogenesis, 9:225–30, 2006.

[35] M. Shibuya. Structure and dual function of vascular endothelial growth factor receptor-1 (Flt-1). Int. J. Biochem. Cell Biol., 33:409–20, 2001.

[36] P. Dalal, W. Muller, and D. Sullivan. Endothelial cell calcium signaling during barrier function and inflammation. Am. J. Pathol., 190, 2019.

[37] V. P. Singh, A. Bali, N. Singh, and A. S. Jaggi. Advanced glycation end products and diabetic complications. Korean J. Physiol. Pharmacol., 18:1–14, 2014.

[38] M. Kanehisa. Post-genome Informatics. Oxford University Press, Kyoto University, Japan, 2000.

[39] T. M. Paravicini and R. M. Touyz. Nadph oxidases, reactive oxygen species, and hypertension clinical implications and therapeutic possibilities. Diabetes care, 31:S170–80, 2008.

[40] N. Koundouros and G. Poulogiannis. Phosphoinositide 3-Kinase/Akt signaling and redox metabolism in cancer. Frontiers in Oncology, 8, 2018.

[41] K. Carranza, D. Veron, A. Cercado, N. Bautista, W. Pozo, A. Tufro, and D. Veron. Cellular and molecular aspects of diabetic nephropathy; the role of VEGF-A. Nefrologia, 35:131–138, 2015.

[42] T. Nakagawa, W. Sato, T. Kosugi, and R. J. Johnson. Uncoupling of VEGF with endothelial NO as a potential mechanism for abnormal angiogenesis in the diabetic nephropathy. Journal of diabetes research, 2013, 2013.

[43] C. M. Warren, S. Ziyad, A. Briot, A. Der, and M. L. Iruela-Arispe. A ligand-independent VEGFR2 signaling pathway limits angiogenic responses in diabetes. Sci. signaling, 7, 2014.

[44] K. S. Yang, J. H. Lim, T. W. Kim, M. Y. Kim, Y. Kim, S. Chung, S. J. Shin, B. S. Choi, H. W. Kim, Y. Kim, Y. S. Chang, H. W. Kim, and C. W. Park. Vascular endothelial growth factor-receptor 1 inhibition aggravates diabetic nephropathy through eNOS signaling pathway in db/db mice. PloS one, 9:e94540, 2014.

[45] D. Feliers, X. Chen, N. Akis, G. G. Choudhury, M. Madaio, and B. S. Kasinath. VEGF regulation of endothelial nitric oxide synthase in glomerular endothelial cells. Kidney Int., 68:1648–59, 2005.

[46] E. Pinter, J. Haigh, A. Nagy, and J. A. Madri. Hyperglycemia-induced vasculopathy in the murine conceptus is mediated via reductions of VEGF-A expression and VEGF receptor activation. Am. J. Pathol., 158:1199–206, 2001.

[47] M. Ferraro. Vascular endothelial growth factor: Basic science and clinical progress. Endocr. Rev., 25:581–611, 2004.

[48] R. Stan, D. Tse, S. Deharvengt, N. Smits, Y. Xu, M. Luciano, C. McGarry, M. Buitendijk, N. Krishnamurthy, R. Elgueta, T. Kobayashi, S. Shipman, K. Moodie, C. Daghlian, P. Ernst, H. Lee, A. Suriawinata, A. Schned, D. Longnecker, and C. Carriére. The diaphragms of fenestrated endothelia: Gatekeepers of vascular permeability and blood composition. Dev. Cell, 23:1203–18, 2012.

[49] H. Prinz. Hill coefficients, dose-response curves and allosteric mechanisms. J Chem Biol., 3:37–44, 2009.

[50] S. Braakman, P. Pathmanathan, and H. Moore. Evaluation framework for systems models. CPT: Pharmacometrics Syst. Pharmacol., 11, 2021.

[51] S Marino, I Hogue, C Ray, and D Kirschner. A methodology for performing global uncertainty and sensitivity analysis in systems biology. J. Theor. Biol., 254:178–196, 2008.

[52] The MathWorks Inc. MATLAB version 9.11.0.1809720 (R2021b) Update 1, 2021. `https://www.mathworks.com/`.

[53] J. Jeong and P. Qiu. Quantifying the relative importance of experimental data points in parameter estimation. BMC Syst. Biol., 12, 2018.

[54] A. Ihler and M. Mandel. Kernel Density Estimation Toolbox for MATLAB (R13), 2007. `https://www.ics.uci.edu/~ihler/code/kde.html`.

[55] S. Yu, Y. Cheng, B. Li, J. Xue, Y. Yin, J. Gao, Z. Gong, J. Wang, and Y. Mu. M1 macrophages accelerate renal glomerular endothelial cell senescence through reactive oxygen species accumulation in streptozotocin-induced diabetic mice. Int. Immunopharmacol., 81:106294, 2020.

[56] T. Nakagawa, W. Sato, Y. Y. Sautin, O. Glushakova, B. Croker, M. A. Atkinson, C. C. Tisher, and R. J. Johnson. Uncoupling of vascular endothelial growth factor with nitric oxide as a mechanism for diabetic vasculopathy. J. Am. Soc. Nephrol., 17:736–45, 2006.

[57] L. F. de Souza, F. Barreto, E. G. da Silva, M. E. Andrades, E. L. M. Guimarães, G. A. Behr, J. F. Moreira, and E. A. Bernard. Regulation of LPS stimulated ros production in peritoneal macrophages from alloxan-induced diabetic rats: Involvement of high glucose and ppar. Life sciences, 81:153–9, 2007.

[58] L. Goers, P. Freemont, and K. Polizzi. Co-culture systems and technologies: Taking synthetic biology to the next level. J. R. Soc. Interface, 11:96, 2014.

[59] N. Kasai, K. Sugimoto, N. Horiba, and T. Suda. Effect of D-glucose on nitric oxide release from glomerular endothelial cells. Diabetes/metabolism research and reviews, 17:217–22, 2001.

[60] S. He, Q. Hu, X. Xu, Y. Niu, Y. Chen, Y. Lu, Q. Su, and L. Qin. Advanced glycation end products enhance m1 macrophage polarization by activating the MAPK pathway. Biochem. Biophys. Res. Commun., 525, 2020.

[61] Z Yang, X Mo, Q Gong, Q Pan, X Yang, W Cai, C Li, J X Ma, Y He, and G. Gao. Critical effect of VEGF in the process of endothelial cell apoptosis induced by high glucose. Apoptosis, 13:1331–43, 2008.

[62] J A Seo, N D Sayyed, Y J Lee, H Y Jeon, E B Kim, S H Hong, S Cho, M Kim, and K S. Ha. Midazolam ameliorates hyperglycemia-induced glomerular endothelial dysfunction by inhibiting transglutaminase 2 in diabetes. Int. J. Mol. Sci., 23:753, 2022.

[63] M. Ramanathan, A. Giladi, and Leibovich J. S. Regulation of vascular endothelial growth factor gene expression in murine macrophages by nitric oxide and hypoxia. Exp Biol. Med., 228:697–705, 2003.

[64] L. Du, F. Dong, L. Guo, H. Yinglong, F. Yi, J. Liu, and D. Xu. Interleukin-1 increases permeability and upregulates the expression of vascular endothelial-cadherin in human renal glomerular endothelial cells. Mol. Med. Rep., 11, 2015.

[65] A. Rohatgi. WebPlotdigitizer: Version 4.4, 2020. `https://automeris.io/WebPlotDigitizer`.

[66] M. D. Abramoff, P. J. Magalhaes, and S. J. Ram. Image processing with imagej. Biophotonics International, 11:36–42, 2004.

[67] S. Makaryan and S. Finley. Enhancing network activation in natural killer cells: predictions from in silico modeling. Integr. Biol., 12:109–121, 2020.

[68] C. Terfve, T. Cokelaer, D. Henriques, A. MacNamara, E. Goncalves, M. K. Morris, M. van Iersel, D. A. Lauffenburger, and J. Saez-Rodriguez. Cellnoptr: A flexible toolkit to train protein signaling networks to data using multiple logic formalisms. BMC Syst. Biol., 6:133, 2012.

[69] R. S. Wang, A. Saadatpour, and R. Albert. Boolean modeling in systems biology: An overview of methodology and applications. Phys. Biol., 9:055001, 2012.

[70] RStudio Team. RStudio: Integrated Development Environment in R, 2020. `http://www.rstudio.com/`.

[71] H. Itaya, T. Imaizumi, H. Yoshida, M. Koyama, S. Suzuki, and K. Satoh. Expression of vascular endothelial growth factor in human monocyte/macrophages stimulated with lipopolysaccharide. Thromb. Haemostasis, 85:171–6, 2001.

[72] J. Rex, U. Albrecht, C. Ehlting, M. Thomas, U. Zanger, O. Sawodny, D. Häussinger, M. Ederer, R. Feuer, and J. Bode. Model-based characterization of inflammatory gene expression patterns of activated macrophages. PLoS Comput. Biol., 12, 2016.

[73] X. Chen, J. Chen, X. Li, and Z. Yu. Activation of mTOR mediates hyperglycemia-induced renal glomerular endothelial hyperpermeability via the RhoA/ROCK/pmlc signaling pathway. Diabetol Metab Syndr, 13, 2021.

Appendix A: Supplementary Information

1. Model Equations

The following model equations govern network interactions. Here, f_{act} and f_{inhib} are the activation and inhibition functions, respectively as defined in the main text. AND and OR logic gate operator is explained as follows: AND logic rule is implemented as multiplicative combinations of activating or inhibiting functions $AND(m, n) = mn$. OR logic rule is computed as $OR(m, n) = m + n–mn$.

$$\frac{\text{dGLU}}{\text{dt}} = \frac{y_{\text{max}_{\text{GLU}}} W_{\text{GLU}} - \text{GLU}}{\tau_{\text{GLU}}} \tag{A1}$$

$$\frac{\text{dLPS}}{\text{dt}} = \frac{y_{\text{max}_{\text{LPS}}} W_{\text{LPS}} - \text{LPS}}{\tau_{\text{LPS}}} \tag{A2}$$

$$\frac{\text{dAGE}}{\text{dt}} = \frac{y_{\text{max}_{\text{AGE}}} f_{\text{act}}(\text{GLU}) - \text{AGE}}{\tau_{\text{AGE}}} \tag{A3}$$

$$\frac{\text{dVEGFR}_1}{\text{dt}} = \frac{y_{\text{max}_{\text{VEGFR}_1}} f_{\text{act}}(\text{VEGFa}) - \text{VEGFR}_1}{\tau_{\text{VEGFR}_1}} \tag{A4}$$

$$\frac{\text{dVEGFR}_2}{\text{dt}} = \frac{y_{\text{max}_{\text{VEGFR}_2}} f_{\text{act}}(\text{VEGFa}) - \text{VEGFR}_2}{\tau_{\text{VEGFR}_2}} \tag{A5}$$

$$\frac{\text{dVEGFR}_{\text{mRNA}}}{\text{dt}} = \frac{y_{\text{max}_{\text{VEGF}_{\text{mRNA}}}} f_{\text{act}}(\text{NFKB}) - \text{VEGF}_{\text{mRNA}}}{\tau_{\text{VEGF}_{\text{mRNA}}}} \tag{A6}$$

$$\frac{\text{dRAGE}}{\text{dt}} = \frac{y_{\text{max}_{\text{RAGE}}} f_{\text{act}}(\text{AGE}) - \text{RAGE}}{\tau_{\text{RAGE}}} \tag{A7}$$

$$\frac{\mathrm{dRAGE_{ec}}}{\mathrm{dt}} = \frac{y_{\mathrm{max_{RAGE_{ec}}}} f_{\mathrm{act}}(\mathrm{AGE}) - \mathrm{RAGE_{ec}}}{\tau_{\mathrm{RAGE_{ec}}}} \tag{A8}$$

$$\frac{\mathrm{dTLR4}}{\mathrm{dt}} = \frac{y_{\mathrm{max_{TLR4}}} f_{\mathrm{act}}(\mathrm{LPS}) - \mathrm{TLR4}}{\tau_{\mathrm{TLR4}}} \tag{A9}$$

$$\frac{\mathrm{dNADPH}}{\mathrm{dt}} = \frac{y_{\mathrm{max_{NADPH}}} f_{\mathrm{act}}(\mathrm{RAGE}) - \mathrm{NADPH}}{\tau_{\mathrm{NADPH}}} \tag{A10}$$

$$\frac{\mathrm{dNADPH_{ec}}}{\mathrm{dt}} = \frac{y_{\mathrm{max_{NADPH_{ec}}}} f_{\mathrm{act}}(\mathrm{RAGE_{ec}}) - \mathrm{NADPH_{ec}}}{\tau_{\mathrm{NADPH_{ec}}}} \tag{A11}$$

$$\frac{\mathrm{dROS}}{\mathrm{dt}} = \frac{y_{\mathrm{max_{ROS}}} OR(f_{\mathrm{act}}(\mathrm{PI3K}), f_{\mathrm{act}}(\mathrm{NADPH})) - \mathrm{ROS}}{\tau_{\mathrm{ROS}}} \tag{A12}$$

$$\frac{\mathrm{dROS_{ec}}}{\mathrm{dt}} = \frac{y_{\mathrm{max_{ROS_{ec}}}} OR(f_{\mathrm{act}}(\mathrm{eNOS}), f_{\mathrm{act}}(\mathrm{NADPH_{ec}})) - \mathrm{ROS_{ec}}}{\tau_{\mathrm{ROS_{ec}}}} \tag{A13}$$

$$\frac{\mathrm{dPI3K}}{\mathrm{dt}} = \frac{y_{\mathrm{max_{PI3K}}} f_{\mathrm{act}}(\mathrm{TLR4}) - \mathrm{PI3K}}{\tau_{\mathrm{PI3K}}} \tag{A14}$$

$$\frac{\mathrm{dAKT}}{\mathrm{dt}} = \frac{y_{\mathrm{max_{AKT}}} f_{\mathrm{act}}(\mathrm{PI3K}) - \mathrm{AKT}}{\tau_{\mathrm{AKT}}} \tag{A15}$$

$$\frac{\mathrm{dPI3K_{ec}}}{\mathrm{dt}} = \frac{y_{\mathrm{max_{PI3K_{ec}}}} OR(f_{\mathrm{act}}(\mathrm{VEGFR_1}), f_{act}(\mathrm{VEGFR_2})) - \mathrm{PI3K_{ec}}}{\tau_{\mathrm{PI3K_{ec}}}} \tag{A16}$$

$$\frac{\mathrm{dAKT_{ec}}}{\mathrm{dt}} = \frac{y_{\mathrm{max_{AKT_{ec}}}} f_{\mathrm{act}}(\mathrm{AKT_{ec}}) - \mathrm{AKT_{ec}}}{\tau_{\mathrm{AKT_{ec}}}} \tag{A17}$$

$$\frac{\mathrm{dNFKB}}{\mathrm{dt}} = \frac{y_{\mathrm{max_{NFKB}}} OR(AND(f_{\mathrm{act}}(\mathrm{TLR4}), f_{\mathrm{act}}(\mathrm{ROS})), f_{\mathrm{act}}(\mathrm{AKT})) - \mathrm{NFKB}}{\tau_{\mathrm{NFKB}}} \tag{A18}$$

$$\frac{\mathrm{dNFKB_{ec}}}{\mathrm{dt}} = \frac{y_{\mathrm{max_{NFKB_{ec}}}} OR(f_{\mathrm{act}}(\mathrm{PLC}), f_{\mathrm{act}}(\mathrm{ROS_{ec}})) - \mathrm{NFKB_{ec}}}{\tau_{\mathrm{NFKB_{ec}}}} \tag{A19}$$

$$\frac{\mathrm{dNO}}{\mathrm{dt}} = \frac{y_{\mathrm{max_{NO}}} OR(f_{\mathrm{act}}(\mathrm{eNOS}), f_{\mathrm{act}}(\mathrm{Ca})) - \mathrm{NO}}{\tau_{\mathrm{NO}}} \tag{A20}$$

$$\frac{\mathrm{dONOO}}{\mathrm{dt}} = \frac{y_{\mathrm{max_{ONOO}}} AND(f_{\mathrm{act}}(\mathrm{NO}), f_{\mathrm{act}}(\mathrm{ROS_{ec}})) - \mathrm{ONOO}}{\tau_{\mathrm{ONOO}}} \tag{A21}$$

$$\frac{\mathrm{deNOS}}{\mathrm{dt}} = \frac{y_{\mathrm{max_{eNOS}}} f_{\mathrm{act}}(\mathrm{AKT_{ec}}) - \mathrm{eNOS}}{\tau_{\mathrm{eNOS}}} \tag{A22}$$

$$\frac{\mathrm{dIL6}}{\mathrm{dt}} = \frac{y_{\mathrm{max_{IL6}}} OR(f_{\mathrm{act}}(\mathrm{NFKB}), f_{\mathrm{act}}(\mathrm{NFKB_{ec}})) - \mathrm{IL6}}{\tau_{\mathrm{IL6}}} \tag{A23}$$

$$\frac{\mathrm{dTNFa}}{\mathrm{dt}} = \frac{y_{\mathrm{max_{TNFa}}} OR(f_{\mathrm{act}}(\mathrm{NFKB}), f_{\mathrm{act}}(\mathrm{NFKB_{ec}})) - \mathrm{TNFa}}{\tau_{\mathrm{TNFa}}} \tag{A24}$$

$$\frac{\mathrm{dIL1b}}{\mathrm{dt}} = \frac{y_{\mathrm{max_{IL1b}}} OR(f_{\mathrm{act}}(\mathrm{NFKB}), f_{\mathrm{act}}(\mathrm{NFKB_{ec}})) - \mathrm{IL1b}}{\tau_{\mathrm{IL1b}}} \tag{A25}$$

$$\frac{\mathrm{dPLC}}{\mathrm{dt}} = \frac{y_{\mathrm{max}_{\mathrm{PLC}}} f_{\mathrm{act}}(\mathrm{VEGFR}_1) - \mathrm{PLC}}{\tau_{\mathrm{PLC}}} \tag{A26}$$

$$\frac{\mathrm{dVEGFa}}{\mathrm{dt}} = \frac{y_{\mathrm{max}_{\mathrm{VEGFa}}} f_{\mathrm{act}}(\mathrm{VEGF}_{\mathrm{mRNA}}) - \mathrm{VEGFa}}{\tau_{\mathrm{VEGFa}}} \tag{A27}$$

$$\frac{\mathrm{dCa}}{\mathrm{dt}} = \frac{y_{\mathrm{max}_{\mathrm{Ca}}} OR(f_{\mathrm{inhib}}(\mathrm{NO}), f_{\mathrm{act}}(\mathrm{PLC})) - \mathrm{Ca}}{\tau_{\mathrm{Ca}}} \tag{A28}$$

$$\frac{\mathrm{dpJunction}}{\mathrm{dt}} = \frac{y_{\mathrm{max}_{\mathrm{pJunction}}} f_{\mathrm{act}}(\mathrm{Ca}) - \mathrm{pJunction}}{\tau_{\mathrm{pJunction}}} \tag{A29}$$

$$\frac{\mathrm{dGapWidth}}{\mathrm{dt}} = \frac{y_{\mathrm{max}_{\mathrm{GapWidth}}} f_{\mathrm{act}}(\mathrm{pJunction}) - \mathrm{GapWidth}}{\tau_{\mathrm{GapWidth}}} \tag{A30}$$

2. Matlab Code

The supporting Matlab code can be found in the Bitbucket respository named *kidneyimmuneLBM* under the *coupledODE extended model* folder.

3. Model Parameter List

In this section, we provide the default list of model parameters by NetFlux. Table A1 and A2 show the list of default species and reaction parameters, respectively. Table A3 provides the list of species with sensitive time constant (τ) parameters and the list of reaction rules corresponding to the sensitive reaction parameters, W, EC_{50}, and n, which were optimized in the model training step.

4. Regulatory species dynamics

We provide the species dynamics of different regulatory species in the network that were not used in model training. The species dynamics capture the behavior of signaling molecules, transcription factor, and receptors for which we

TABLE A1. Default species parameters. Initial value (y_0), maximum value ($y_{\max}$), and time constant (τ) for respective species in the model. The unit for τ is in hour.

Species	y_0	$y_{\max}$	τ (h)
GLU	0	1	1
LPS	0	1	1
AGE	0	1	1
$VEGFR_1$	0	1	1
$VEGFR_2$	0	1	1
$VEGFa_{mRNA}$	0	1	1
$RAGE_{ec}$	0	1	1
$RAGE$	0	1	1
$TLR4$	0	1	1
$NADPH$	0	1	1
$NADPH_{ec}$	0	1	1
ROS_{ec}	0	1	1
ROS	0	1	1
$PI3K$	0	1	1
AKT	0	1	1
$PI3K_{ec}$	0	1	1
AKT_{ec}	0	1	1
$NFKB_{ec}$	0	1	1
$NFKB$	0	1	1
NO	0	1	1
$ONOO$	0	1	1
$eNOS$	0	1	1
$IL6$	0	1	1
$TNF\alpha$	0	1	1
$IL1\beta$	0	1	1
$PLC\gamma$	0	1	1
$VEGFa$	0	1	1
$pJunction$	0	1	1
Ca	0	1	1
$GapWidth$	0	1	1

could not obtain experimental data. Fig. A3, A4, and A5 captures the species expression over 48 hours under glucose only, LPS only, and glucose and LPS treatment, respectively.

TABLE A2. Default reaction parameters. Reaction weight (W), Hill coefficient (n), and half effect (EC_{50}) for respective reaction rules in the model.

Index	**Reaction Rule**	W	n	EC_{50}
1	$=>GLU$	0	1.4	0.5
2	$=>LPS$	0	1.4	0.5
3	$LPS=>TLR4$	1	1.4	0.5
4	$GLU=>AGE$	1	1.4	0.5
5	$AGE=>RAGE$	1	1.4	0.5
6	$RAGE=>NADPH$	1	1.4	0.5
7	$TLR4\ \&\ ROS=>NFKB$	1	1.4	0.5
8	$TLR4=>PI3K$	1	1.4	0.5
9	$NADPH=>ROS$	1	1.4	0.5
10	$PI3K=>AKT$	1	1.4	0.5
11	$PI3K=>ROS$	1	1.4	0.5
12	$NFKB_{ec}=>TNF\alpha$	1	1.4	0.5
13	$AKT=>NFKB$	1	1.4	0.5
14	$NFKB=>IL6$	1	1.4	0.5
15	$NFKB=>TNF\alpha$	1	1.4	0.5
16	$NFKB=>VEGFa_{mRNA}$	1	1.4	0.5
17	$VEGFa_{mRNA}=>VEGFa$	1	1.4	0.5
18	$NFKB=>IL1\beta$	1	1.4	0.5
19	$VEGFa=>VEGFR_1$	1	1.4	0.5
20	$VEGFa=>VEGFR_2$	1	1.4	0.5
21	$AGE=>RAGE_{ec}$	1	1.4	0.5
22	$RAGE_{ec}=>NADPH_{ec}$	1	1.4	0.5
23	$VEGFR_2=>PI3K_{ec}$	1	1.4	0.5
24	$VEGFR_1=>PI3K_{ec}$	1	1.4	0.5
25	$NADPH_{ec}=>ROS_{ec}$	1	1.4	0.5
26	$PI3K_{ec}=>AKT_{ec}$	1	1.4	0.5
27	$AKT_{ec}=>eNOS$	1	1.4	0.5
28	$VEGFR_1=>PLC\gamma$	1	1.4	0.5
29	$PLC\gamma=>NFKB_{ec}$	1	1.4	0.5
30	$ROS_{ec}=>NFKB_{ec}$	1	1.4	0.5
31	$NFKBe_{ec}=>IL6$	1	1.4	0.5
32	$NFKBe_{ec}=>IL1\beta$	1	1.4	0.5
33	$eNOS=>NO$	1	1.4	0.5
34	$eNOS=>ROS_{ec}$	1	1.4	0.5
35	$ROS_{ec}\ \&\ NO=>ONOO$	1	1.4	0.5
36	$!NO=>Ca$	1	1.4	0.5
37	$PLC\gamma=>Ca$	1	1.4	0.5
38	$Ca=>pJunction$	1	1.4	0.5
39	$pJunction=>GapWidth$	1	1.4	0.5
40	$Ca=>NO$	1	1.4	0.5

TABLE A3. List of species and reaction rules that correspond to sensitive parameter subspace are given. Sensitive time constant (τ) parameters for respective species are provided. Sensitive reaction parameters such as Hill coefficient (n), half effect (EC_{50}), and reaction weight (W) for respective reaction rule are provided. Reaction rule $A\&B => C$ indicates that an AND logic operator between input A and input B gives output C. Reaction rule $A => C$ indicates that input A gives output C.

Species	**Reaction Rule**		
τ (h)	n	EC_{50}	W
τ_{GLU}	$TLR4$ & $ROS => NFKB$	$AKT_{ec} => eNOS$	$VEGFa => VEGFR_2$
τ_{LPS}	$NFKB_{ec} => TNF\alpha$	$eNOS => NO$	$VEGFR_1 => PI3K_{ec}$
τ_{RAGE}	$NFKB => IL1\beta$	$NFKB_{ec} => IL6$	$PI3K_{ec} => AKT_{ec}$
τ_{NADPH}	$AKT_{ec} => eNOS$	$TLR4$ & $ROS => NFKB$	$AKT_{ec} => eNOS$
τ_{NFKB}	$eNOS => NO$	$TLR4 => PI3K$	$eNOS => NO$
τ_{NO}	ROS_{ec} & $NO => ONOO$		
τ_{eNOS}	$LPS => TLR4$		
	$PI3K => ROS$		
	$VEGFa => VEGFR_2$		
	$AGE => RAGE_{ec}$		
	$PLC\gamma => NFKB_{ec}$		
	$ROS_{ec} => NFKB_{ec}$		

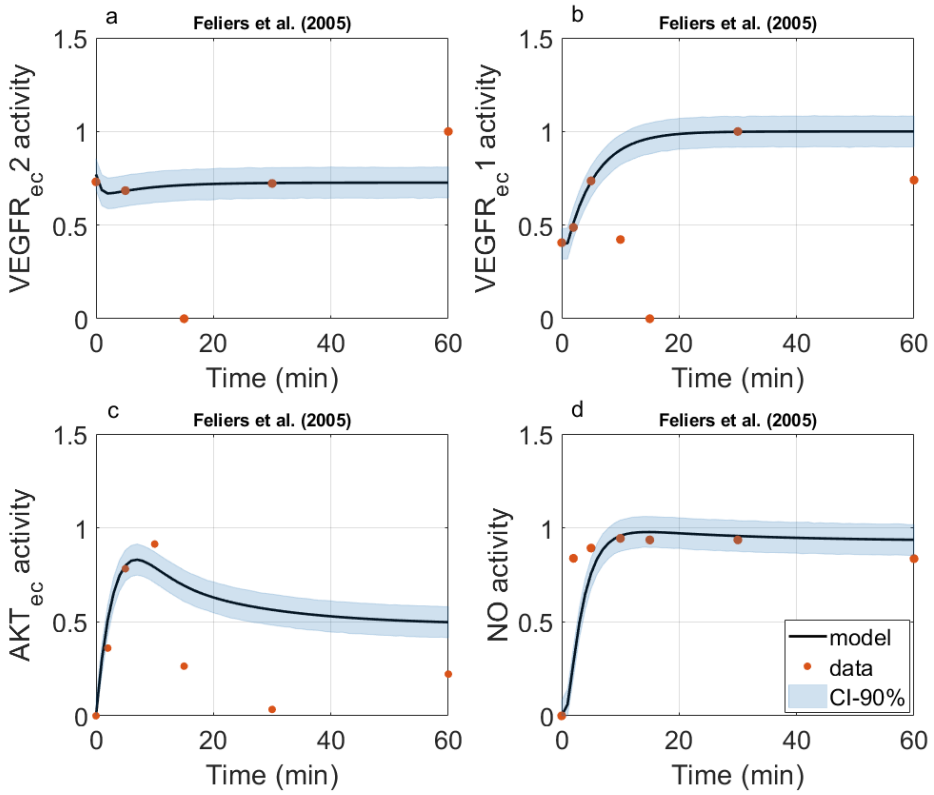

FIG. A1. Simlations from a single cell network model of glomerular endothelial cells stimulated with *LPS* only treatment. These simulations were in absence of macrophage cells and were simulated for 60 minutes with LPS-dependent VEGF to mimic experimental model [45]. This simulation allowed us to estimate parameters that capture the discrepancies VEGF-mediated VEGFR-1 and VEGFR-2 signaling. Black curves are mean predictions, orange points are data from Feliers et al. [45], blue shaded regions are 90% confidence regions.

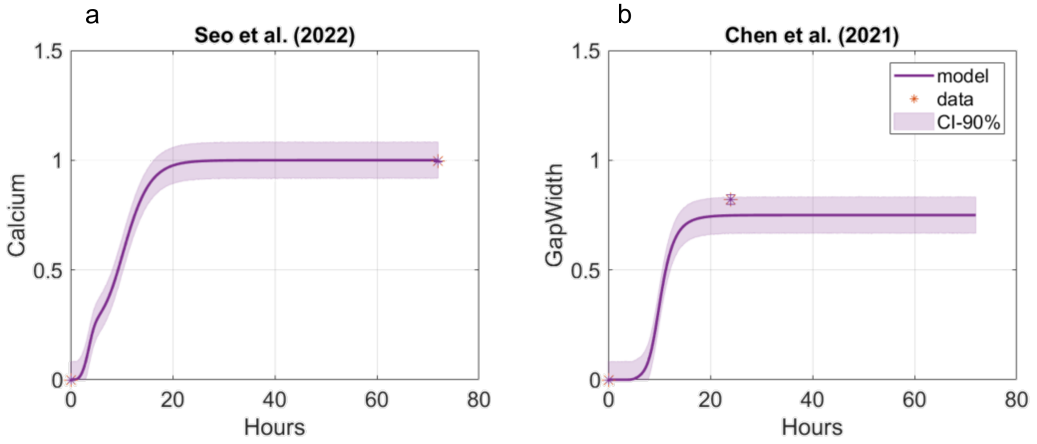

FIG. A2. Network responses, intracellular calcium in glomerular endothelial cell culture and intercellullar fenestration or gap with in glomerular endothelial cells (GEC) are validated under high glucose. (a) Calcium activity predicted over 72 hours is compared against fold change intracellular calcium data from Seo *et al.* [62]. (b) Gap Width is the predicted change in intercellular gaps between GECs upon high glucose stimulation. The predicted gap width change is compared against change in gap size (area) in GECs from Chen *et al.* [73].

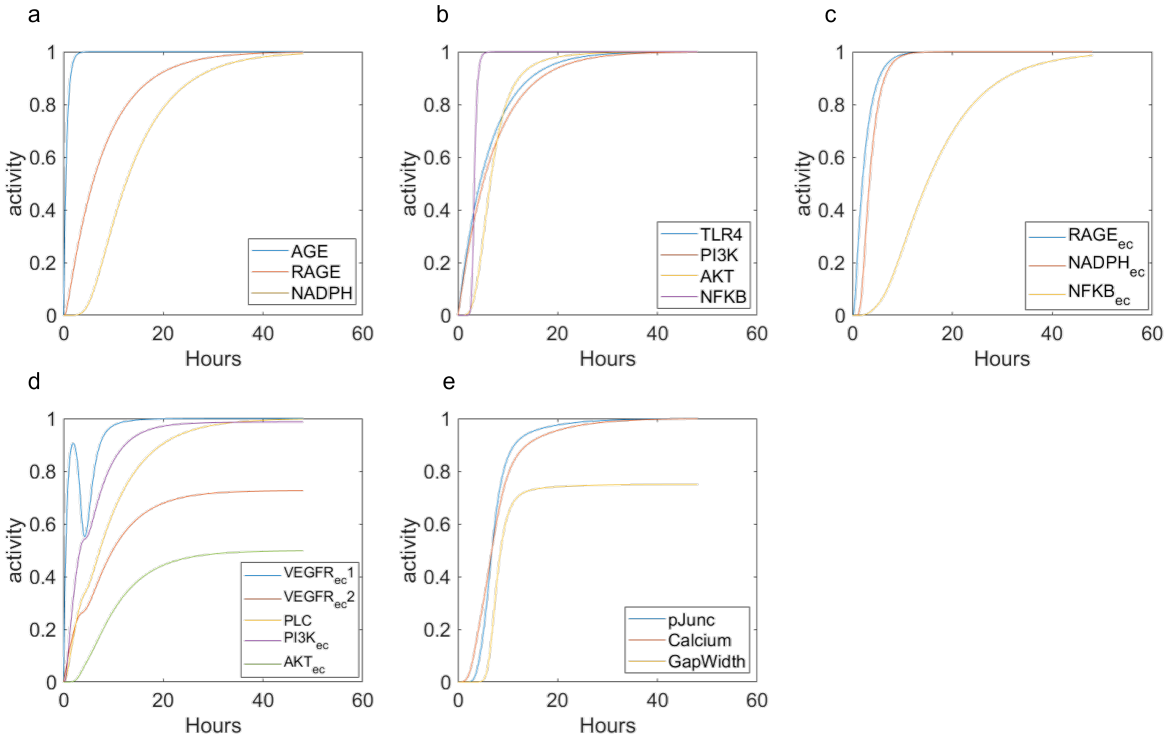

FIG. A3. Species activity over 48 hours for all regulatory species in the network when stimulated with *GLU* are shown. (a)-(e) show dynamics of species grouped by interactions in a sub-network as mentioned in respective legend. pJunc is the pJunction node in the network. "ec" subscript denotes intercellular species within glomerular endothelial cells in the network.

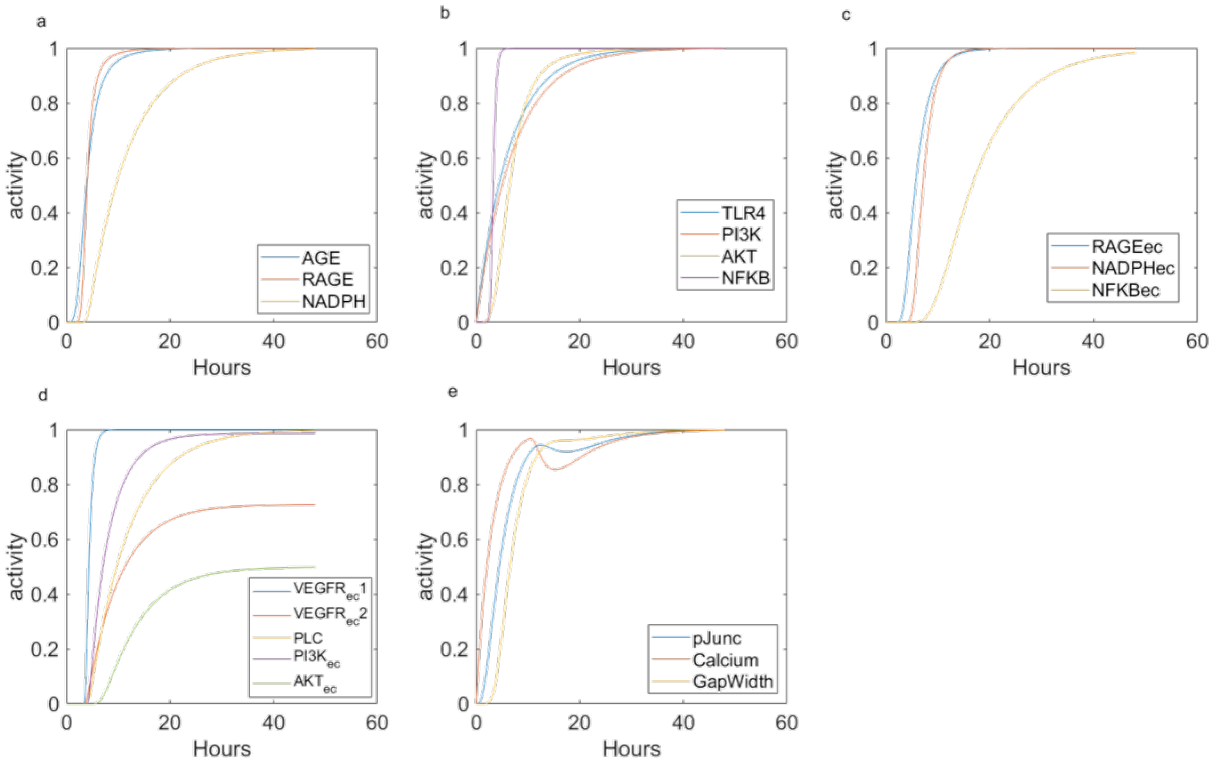

FIG. A4. Species activity over 48 hours for all regulatory species in the network when stimulated with *LPS* are shown. (a)-(e) show dynamics of species grouped by interactions in a sub-network as mentioned in respective legend. pJunc is the pJunction node in the network. "ec" subscript denotes intercellular species within glomerular endothelial cells in the network.

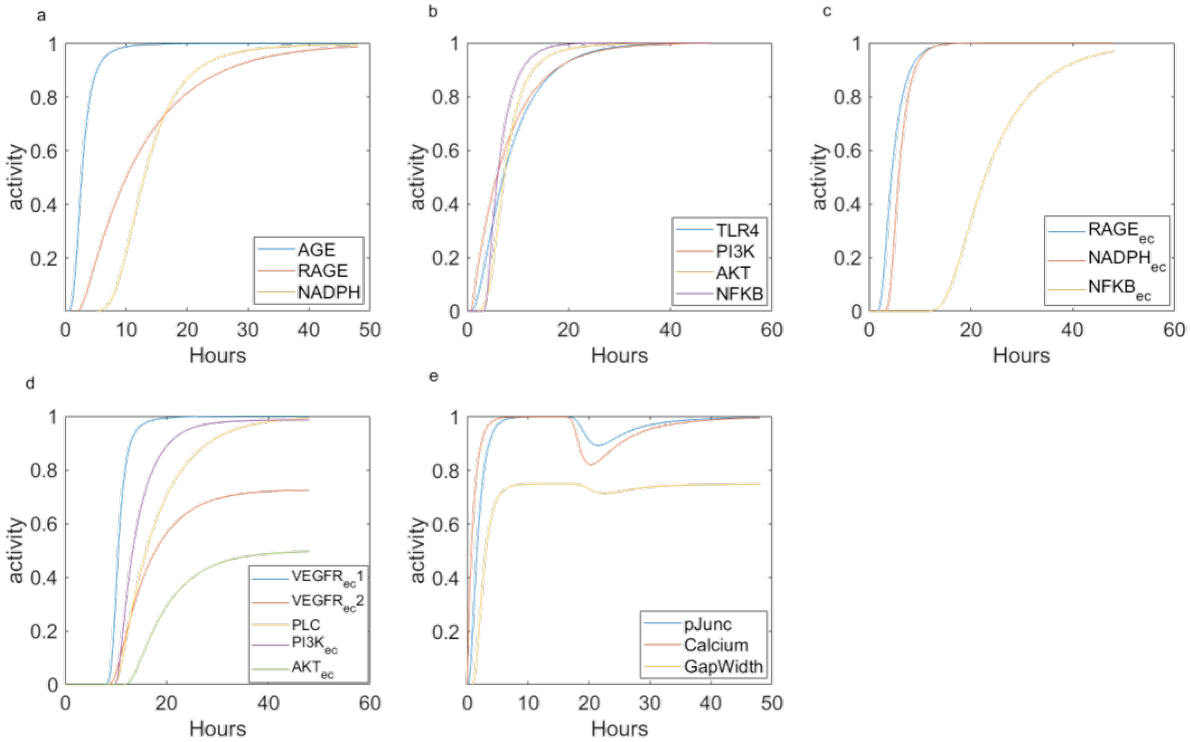

FIG. A5. Species activity over 48 hours for all regulatory species in the network when stimulated with *GLU* and *LPS* are shown. (a)-(e) show dynamics of species grouped by interactions in a sub-network as mentioned in respective legend. pJunc is the pJunction node in the network. "ec" subscript denotes intercellular species within glomerular endothelial cells in the network.

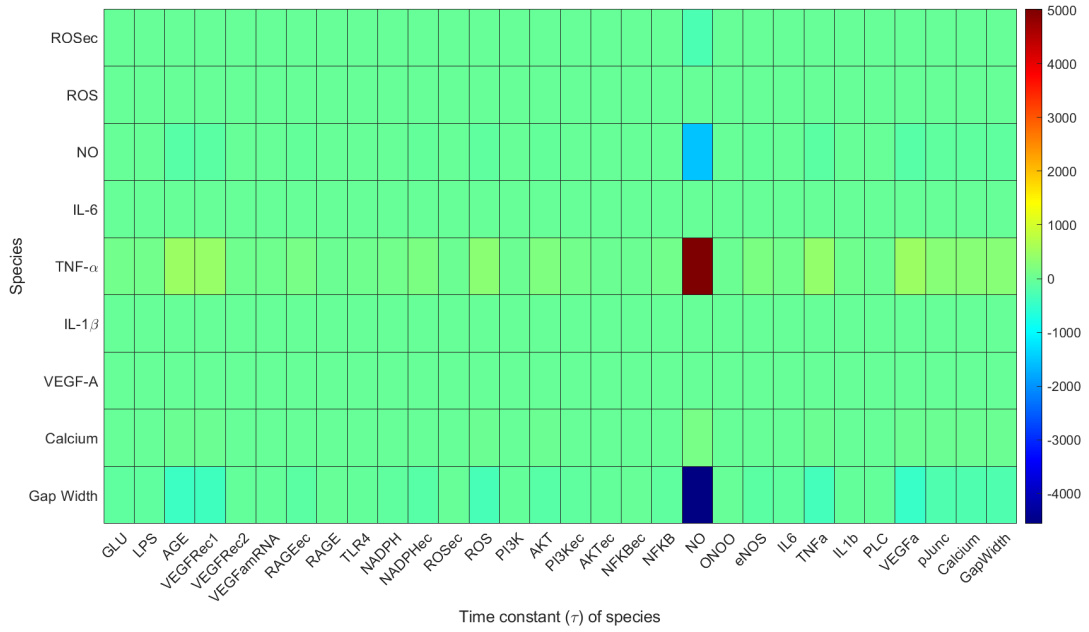

FIG. A6. The local sensitivity coefficient of change in output species (vertical axis) against the change in τ parameters (horizontal axis) is given as a heatmap. Color bar indicates the magnitude of the sensitivity coefficient.

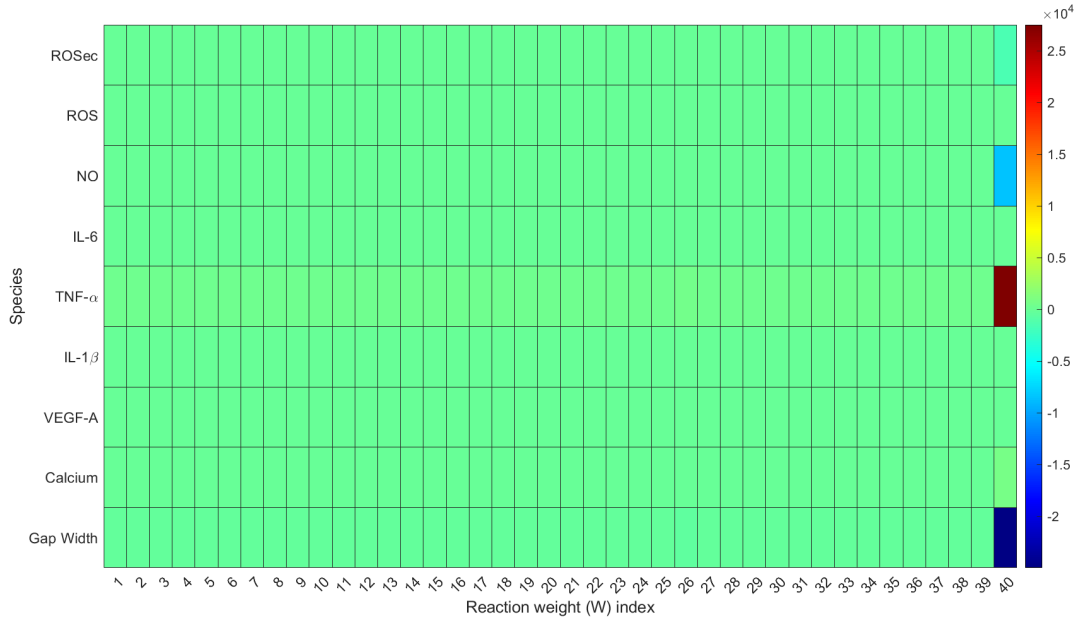

FIG. A7. The local sensitivity coefficient of change in output species (vertical axis) against the change in W parameters (horizontal axis) is given as a heatmap. Index for each W parameter corresponds to an interaction rule. Refer to Table A2. Color bar indicates the magnitude of the sensitivity coefficient.

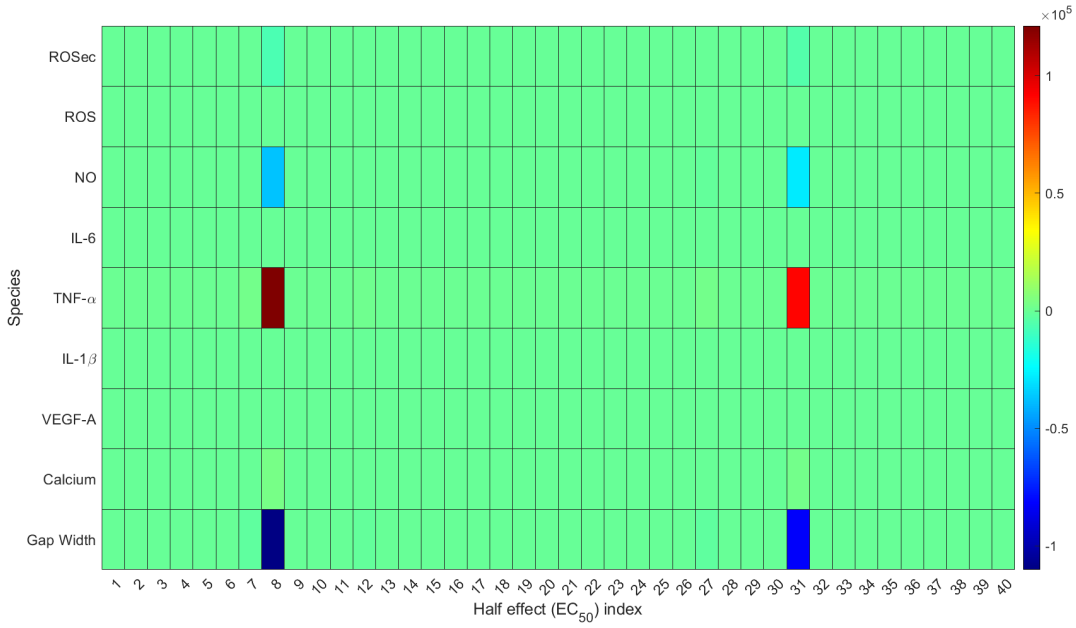

FIG. A8. The local sensitivity coefficient of change in output species (vertical axis) against the change in EC_{50} parameters (horizontal axis) is given as a heatmap. Index for each EC_{50} parameter corresponds to an interaction rule. Refer to Table A2. Color bar indicates the magnitude of the sensitivity coefficient.